

# Recent Advances on Cell Culture Platforms for In Vitro Drug Screening and Cell Therapies: From Conventional to Microfluidic Strategies

Beatriz D. Cardoso, Elisabete M. S. Castanheira, Senentxu Lanceros-Méndez, and Vanessa F. Cardoso\*

The clinical translations of drugs and nanomedicines depend on coherent pharmaceutical research based on biologically accurate screening approaches. Since establishing the 2D in vitro cell culture method, the scientific community has improved cell-based drug screening assays and models. Those advances result in more informative biochemical assays and the development of 3D multicellular models to describe the biological complexity better and enhance the simulation of the in vivo microenvironment. Despite the overall dominance of conventional 2D and 3D cell macroscopic culture methods, they present physicochemical and operational challenges that impair the scale-up of drug screening by not allowing a high parallelization, multidrug combination, and high-throughput screening. Their combination and complementarity with microfluidic platforms enable the development of microfluidics-based cell culture platforms with unequivocal advantages in drug screening and cell therapies. Thus, this review presents an updated and consolidated view of cell culture miniaturization's physical, chemical, and operational considerations in the pharmaceutical research scenario. It clarifies advances in the field using gradient-based microfluidics, droplet-based microfluidics, printed-based microfluidics, digital-based microfluidics, SlipChip, and paper-based microfluidics. Finally, it presents a comparative analysis of the performance of cell-based methods in life research and development to achieve increased precision in the drug screening process.

## 1. Introduction

Microfluidics is the term used to describe the science and technology that deals with the fabrication of miniaturized devices and the manipulation of fluids ( $10^{-9}$ – $10^{-18}$  L) confined in channels with dimensions in the micrometer range.<sup>[1]</sup> The embrace of microfluidics technology as it is recognized today was introduced in 1990<sup>[2]</sup> by the term “miniaturized total chemical analysis systems”— $\mu$ TAS—which defines a single device that comprises multiple laboratory steps. The basic concept of  $\mu$ TAS is based on the transformation of (bio)chemical information (such as the activity of particles and chemical concentrations) into electronic data in a fully automated system with the size of a chip.<sup>[2]</sup> The cumulative comprehension of the behavior and control of fluid flow at the microscale allowed the rapid advancement of this area.<sup>[3]</sup> As a result, the state-of-the-art integrates several review articles that explore concepts such as the fluidic behavior in a variety of devices,<sup>[4]</sup> the physics behind the fluid phenomena,<sup>[5]</sup> the fundamental kinematics of microparticles

B. D. Cardoso, E. M. S. Castanheira, S. Lanceros-Méndez  
Physics Centre of Minho and Porto Universities (CF-UM-UP), Campus de Gualtar

University of Minho  
Braga 4710-057, Portugal

B. D. Cardoso, E. M. S. Castanheira, S. Lanceros-Méndez  
LaPMET-Laboratory of Physics for Materials and Emergent Technologies  
University of Minho  
4710-057 Braga, Portugal

B. D. Cardoso, V. F. Cardoso  
Center for MicroElectromechanical Systems (CMEMS-UMinho)  
Campus de Azurém


University of Minho  
4800-058 Guimarães, Portugal  
E-mail: vcardoso@cmems.uminho.pt

B. D. Cardoso, V. F. Cardoso  
LABBELS-Associate Laboratory in Biotechnology and Bioengineering and  
Microelectromechanical Systems

University of Minho  
Braga/Guimarães Portugal

S. Lanceros-Méndez  
BCMaterials  
Basque Center for Materials  
Applications and Nanostructures  
UPV/EHU Science Park  
Leioa 48940, Spain

S. Lanceros-Méndez  
IKERBASQUE  
Basque Foundation for Science  
Bilbao 48009, Spain

 The ORCID identification number(s) for the author(s) of this article can be found under <https://doi.org/10.1002/adhm.202202936>

© 2023 The Authors. Advanced Healthcare Materials published by Wiley-VCH GmbH. This is an open access article under the terms of the Creative Commons Attribution-NonCommercial License, which permits use, distribution and reproduction in any medium, provided the original work is properly cited and is not used for commercial purposes.

DOI: 10.1002/adhm.202202936

inside microchannels,<sup>[6]</sup> and the small-scale mixing,<sup>[7]</sup> among others.

Furthermore, the versatility of microfluidic devices in integrating multiple components (e.g., micropumps, mixers, separation columns, reactors)<sup>[8]</sup> and their combination with existing macrodevices makes them excellent for high parallelization.<sup>[9]</sup> The knowledge consolidation combined with the technology's stated potential has allowed it to extend its applicability to several fields.<sup>[10]</sup> As a result, microfluidics is currently implemented in the analysis of residual antibiotics in food,<sup>[11]</sup> production of monodisperse emulsions in cosmetics,<sup>[12]</sup> fertility testing,<sup>[13]</sup> monitoring of blood glucose,<sup>[14]</sup> and onsite environmental detection,<sup>[15]</sup> as representative examples. Among the different application possibilities, healthcare is one of the fields that can take the most advantage of microfluidics in the entire spectrum of research, development, diagnosis, and therapeutics. The societal and economic impact of several diseases requires accelerating the clinical translation of nanomedicines and drugs in a research and development line that allows a more precise, faster, and accurate discovery and evaluation. In this aspect, microfluidics can be highly beneficial for the initial drug discovery stage, especially for production and screening using cell-based platforms.

The establishment of *in vitro* cell culture<sup>[16]</sup> is still one of the breakthroughs of the 20<sup>th</sup> century. Conventional 2D cell culture is a laboratory approach in pharmaceutical research and fills the knowledge gap between biochemical assays and animal model testing.<sup>[17]</sup> Although 2D cell culture is an informative and relevant approach, the microenvironment in the conventional cell culture plates distances itself from physiological conditions, making this method simplistic in describing the biological complexity.<sup>[18]</sup> Additionally, testing in animal models raises ethical and monetary issues.<sup>[19]</sup> As a result, 3D cell culture has asserted its importance in cell biology research, providing a platform that ensures an enhanced simulation of the *in vivo* microenvironment and its complex interactions.<sup>[20]</sup>

Although the advantages of conventional 2D and 3D cell culture in pharmaceutical research should not be overlooked, they face challenges that lead to misleading information resulting in inconsistent *in vivo* responses.<sup>[17]</sup> Thus, the window of opportunities and accuracy of cell culture methods (2D and 3D) can be widened through their convergence with microfluidic platforms. The use of microfluidics-based 2D and 3D cell culture systems that better mimic *in vivo* microenvironments and dynamic fluid flow conditions enable access to mechanisms and physical phenomena that would otherwise become unnoticed. Furthermore, the reproducible and quicker screening of drugs at an early stage of development can actively contribute to reducing the late-stage failure risk while reducing animal experimentation.<sup>[21]</sup> The accurate validation of new medicines can be thus supported by understanding how microenvironments created on microfluidic platforms influence cellular behavior and functions and how those microenvironments can be adjusted for better *in vitro* control. As a result, relevant review articles address the technical challenges that limit the widespread accessibility of microfluidics,<sup>[22]</sup> the understanding of molecular and cell biology that can be enhanced by precision microfluidic approaches,<sup>[23]</sup> as well as the role of microfluidics in high-throughput drug screening applications.<sup>[24]</sup> Furthermore, recent literature explores the appli-

cation of microfluidic devices in anticancer and personalized cancer drug screening,<sup>[25]</sup> organoid-based disease models combined with microfluidics,<sup>[26]</sup> as well as the advances in the application of specific types of microfluidic devices in biomedicine, such as single-cell droplet microfluidics,<sup>[27]</sup> and concentration gradient microfluidics.<sup>[28]</sup>

In this context, the present review represents an update to the current literature by addressing the most relevant practical considerations of the topics mentioned above while explicitly highlighting cell culture's essential role in drug screening. It explores the advantages that make 2D and 3D cell culture relevant methods in the drug research scenario and the challenges that limit them from being more effective in drug validation. Furthermore, the complementarity of cell culture methods with microfluidic platforms toward a more reliable and simplified drug screening is also explored. For that, this work describes the most relevant physicochemical and operational considerations that miniaturization entails and how this technology represents a suitable approach for *in vitro* control of cells' physiological context. Finally, recent advances in the area highlight the prospects of microfluidics-based cell culture devices for drug screening and cell therapies. Relevant works are reviewed using gradient-based microfluidics, droplet-based microfluidics, printed-based microfluidics, digital-based microfluidics, SlipChip, and paper-based microfluidics.

## 2. Life Science Research and Development: An Overview of Cell Culture as a Model for Drug Screening

Healthcare is highly dependent on drug research and development; therefore, it is essential to promote drug innovation on an ongoing basis. The human body is a highly dynamic, multilevel, and complex biological system, hindering the accurate prediction of a drug's entire spectrum of influences and effects. The drug discovery paradigm must be continuously updated due to its social impact. It is also an estimated time- and money-consuming process that typically takes over 12 years or longer from the target identification until the market approval.<sup>[29]</sup>

The complex, lengthy, and expensive process requires methodic planning, which Mohs and Greig<sup>[30]</sup> summarized in a list of individual laboratory contributions to drug discovery and development (**Figure 1**). It is organized as follows: i) target identification; ii) target validation; iii) finding new molecule; iv) screening assays; v) data on drug-like characteristics; vi) development tools; vii) efficacy measures; and viii) technologies to improve the efficiency of trial completion.<sup>[30]</sup> However, there is no predefined key to success, and stepping back in the development line is often necessary. Actually, in cancer's therapeutical area, the overall success rate for products in clinical development is approximately 10%.<sup>[31]</sup> Understanding the reasons for the failure requires efficient collaborations between different expertise areas (e.g., toxicology, biology, physics, and chemistry).<sup>[32]</sup> This knowledge must be followed by a continuous review (or even renewal) of the production processes, analysis, and quantification techniques.

Despite advances in the area, pharmaceutical research is inseparable from cell culture techniques as an essential approach



1. Target identification
2. Target validation
3. Finding new molecule
4. Screening assays
5. Data on drug-like characteristics
6. Development tools
7. Efficacy measures
8. Technologies to improve efficiency of trial completion

**Figure 1.** Schematic representation of the drug discovery process from basic research (initiated by target identification) to its translation into Food and Drug Administration (FDA)-approved product. The arrows represent the quality assurance guides that guarantee the normal development of the process. The “good laboratory practice” are summarized in a list of individual laboratory contributions to drug discovery and development.

to drug discovery. Cell culture techniques are ubiquitously used to discover drug efficacy, delivery, pharmacological actions, and cytotoxicity upon developing and characterizing nanomedicines. Cell cultures have been used for over a century to understand *in vivo* cell behavior and its mechanisms.<sup>[33]</sup> Cell-based assays are one of the most comprehensive approaches to data-harvest quantitative and physiologically relevant information in drug-screening processes.<sup>[34]</sup> The daily scientific articles evidence this relevance, showing its role in research and development. It is estimated that \$135 billion<sup>[35]</sup> is spent yearly on screening medicines. As an *in vitro* model, the cells used in cell-based assays must accurately represent the system to be studied and express relevant factors and signaling intermediates.<sup>[34b]</sup> Most cell-based assays are based on 2D models performed on multiwell plates that are easily monitored.<sup>[36]</sup> Some limitations of 2D cell cultures, such as the difficulties of the multiwell plates in representing the 3D structure of tissues *in vivo*, limit the ability of this method to predict the clinical response of drugs.<sup>[20,37]</sup> Considering that each model reflects different cellular organizational levels and behaviors, the extrapolated information of the screened drug (such as toxicity, safety, and physiological action) depends on the method used. In the following section, some considerations for using 2D and 3D cell cultures in drug screening are detailed, as well as their respective advantages and challenges.

## 2.1. 2D Cell Culture Methods

The conventional cell culture is commonly referred to as 2D due to its inherent dependence on adhesion to a planar and rigid surface, which provides mechanical support for anchorage-dependent cells (meaning that cells need to adhere to a solid) in a monolayer. Besides the well-established methods for cul-

turing, expanding, differentiating, and de-differentiating cells, 2D cell culture is also a simple and relatively low-cost maintenance method.<sup>[38]</sup> Furthermore, this method ensures a homogeneous growth and proliferation of cells since the monolayer cells have uniform access to the components of the medium (such as growth factors and nutrients).<sup>[39]</sup>

Although it remains the most used *in vitro* study model worldwide, it has been showing significant limitations that compromise the achievement of reliable biomedical information. These limitations are mainly due to monolayer cultures' inability to simulate the *in vivo* microenvironment and the cellular architecture. As an example, Weaver et al.<sup>[40]</sup> demonstrated that tissue architecture could regulate the mammary epithelial cells (MECs) sensitivity to exogenous apoptotic stimuli. The authors used nonmalignant S-1 cells of MECs and their tumorigenic progeny (T4-2) grown as 2D monolayers on a thin coat of collagen I, and their respective 3D structures embedded in the reconstituted basement membrane (rBM). Nonmalignant cells formed growth-arrested 3D organoids (acini), while malignant MECs continued to proliferate to form nonpolar, multicellular, and disorganized 3D aggregates (**Figure 2A**). One of the trials aimed to test whether the presence of BM and malignant transformation can modulate the extracellular matrix (ECM) sensitivity to apoptotic stimuli. For that, the authors measured the apoptotic labeling indices of the cell cultures when treated with different apoptotic agents (**Figure 2B**). The results of apoptotic sensitivity of cell cultures grown as 2D monolayers revealed similar responses in all apoptotic agents. In turn, the nonmalignant MEC acini were the only cell cultures demonstrating apoptosis resistance, while the nonmalignant MEC acini showed no apoptosis resistance after malignant transformation. Furthermore, the ligand-activated  $\beta 4$  integrin induces tissue polarity in mammary epithelial acini, and it is involved in apoptosis resistance to several chemical and receptor-linked stimuli.<sup>[40]</sup> These differences are reflected

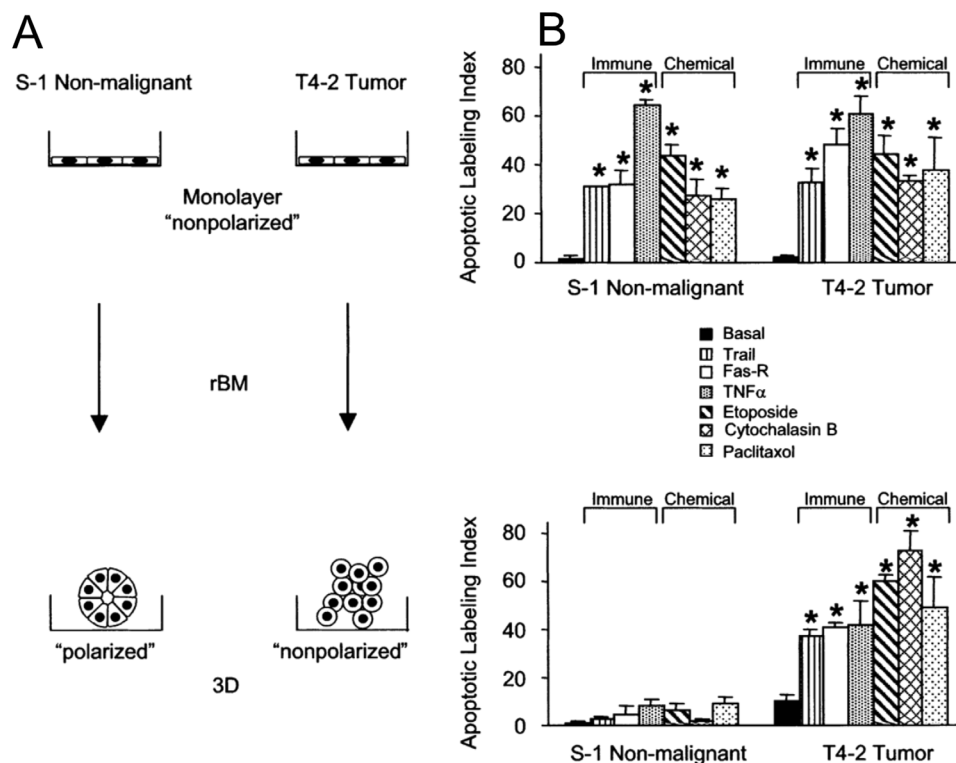


**Figure 2.** A) Schematic representation of non-malignant MECs and malignant MECs treated as monolayers on a thin coat of collagen (above) and their 3D structures embedded in rBM; and their respective, B) apoptotic labeling indices treated with Trail peptide ( $1 \mu\text{g mL}^{-1}$ ), anti-FAS mAb (IgM CH-11,  $2 \mu\text{g mL}^{-1}$ ), TNF- $\alpha$  ( $100 \times 10^{-9} \text{ M}$ ), etoposide ( $50 \times 10^{-6} \text{ M}$ ), cytochalasin B ( $1 \times 10^{-6} \text{ M}$ ), or paclitaxel ( $120 \times 10^{-9} \text{ M}$ ). Results are the mean  $\pm$  SEM of 3–5 separate experiments, each with duplicates or triplicates. Adapted with permission.<sup>[40]</sup> Copyright 2002, Cell Press.

in profound changes regarding their proliferation, cell–cell connections, cell–matrix connections, migration, survival, adhesion, and differentiation.<sup>[41]</sup>

Monolayer cultures do not allow the simulation of oxygen or nutrient gradients that occur naturally in vivo and highly influence cell behavior (cell migration, cell signaling, and cell motility).<sup>[42]</sup> Furthermore, ECM proteins (composed of around 300 different proteins in mammals) play a significant role in mediating cellular functions.<sup>[43]</sup> In addition to the ECM, in vivo cells are also in contact with stromal cells, which include glial cells (in neuronal tissue), mesenchymal supporting cells (in epithelial tissue), immune system cells, and cells of the surrounding vasculature.<sup>[41b]</sup> Regarding cancer drug research, the extrapolated biomedical information from 2D cell cultures is subject to more inconsistencies due to the inherently complex nature of the tumor microenvironment. It consists of a heterogeneous mixture of tumor and stromal cells that, in turn, include growth factors, macrophages, cytokines, and inflammatory cells.<sup>[44]</sup> Cancer-associated fibroblasts (CAFs) are a component with significant abundance in the tumor stroma,<sup>[42]</sup> presenting highly significant tumor-restraining/promoting roles, such as CAF-mediated therapy resistance and tumor progression (for detailed information, see ref. [45]). One of the mechanisms involved in CAF-mediated therapy resistance is the release of cytokines under therapeutic pressure, which activates different signaling cascades in tumor cells. The deoxyribonucleic acid (DNA) damage of CAFs induced by chemotherapeutic drugs has already been shown to trig-

ger a boost of prosurvival pathways in tumor cells. In addition, CAFs support cancer stem cells (CSC) in maintaining stemless features.<sup>[46]</sup> CSCs have a slow-cycling or quiescent state (meaning the cell division process is interrupted), which makes them resistant to chemotherapy drugs which usually target dividing cells.<sup>[47]</sup> As 2D cell cultures cannot review all these contexts, this method is shown to modify their transcriptional regulation, receptor expression, cell invasion,<sup>[48]</sup> cell proliferation, apoptosis, and anti-apoptosis.<sup>[49]</sup>

Some strategies have been used to create models that recapitulate cell behavior in vivo to provide control of cell shape in 2D cell culture. Those techniques include cell-patterning methods, tailoring of substrate stiffness, and sandwich culture. In cell patterning, the conventional homogeneous surface that cells adhere to and grow is replaced by an engineered geometric surface with variable microtopography, allowing control of the size and shape of cells.<sup>[50]</sup> Cell patterning techniques are divided into physical methods<sup>[51]</sup> and biochemical methods.<sup>[52]</sup> These strategies have been used to study fundamental principles of cell biology (such as differentiation, proliferation, and migration)<sup>[53]</sup> and in drug screening.<sup>[54]</sup> In addition, since most tissue cells are anchorage-dependent,<sup>[55]</sup> the stiffness of substrates also influences cell behavior.<sup>[56]</sup> Stiffness variation in cell culture has been shown, for instance, to regulate cell behavior and the resulting chondrogenic fate of human mesenchymal stem cells (MSC) and cartilage phenotype,<sup>[57]</sup> as well as in the regenerative response of neural stem cells.<sup>[58]</sup>



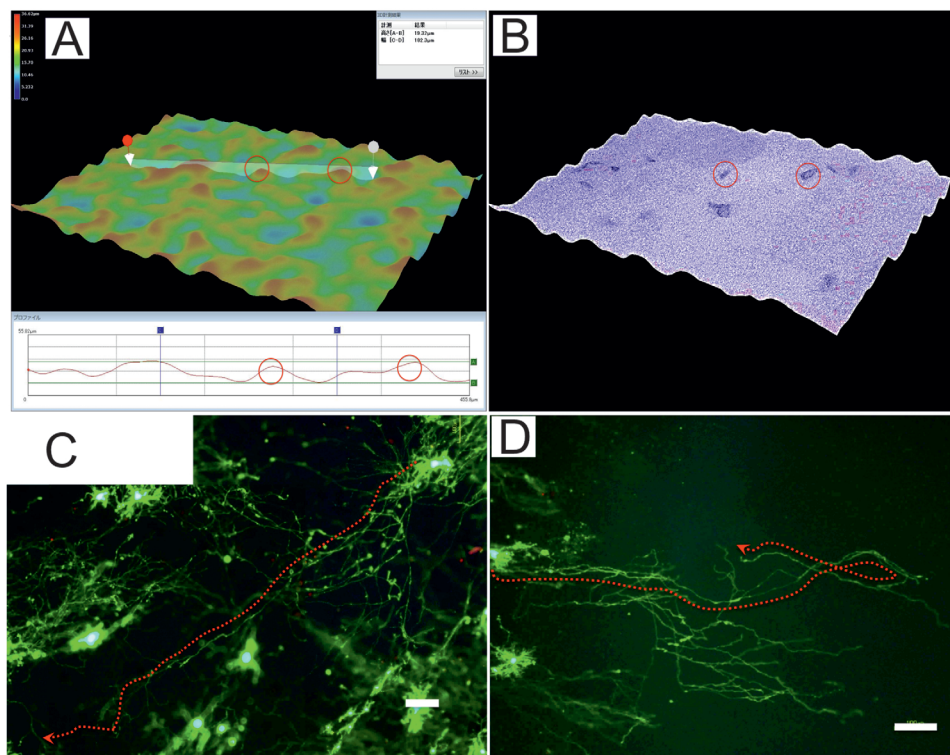


**Figure 3.** A) 3D image of the surface roughness of PuraMatrix with the highest positions displayed in red and the lowest positions in blue (see the color scale at the upper left); and the respective B) high contrast 3D image of primary neurons (dark color) cultivated on that surface. C) Fluorescence images of long-term living cells of 3D growth of neurites at the rough surface of 25% PuraMatrix at  $3 \times 10^4$  cells  $\text{mL}^{-1}$  and coverslipped 3 h after plating (C), or not (D). Bars: 100  $\mu\text{m}$ . Both A and B show long neurites ( $> 1600 \mu\text{m}$ , arrows). Adapted under the terms of the CC-BY-4.0 license.<sup>[62a]</sup> Copyright 2014, the Authors. Published by PloS One.

The sandwich culture was proposed by Dunn et al.<sup>[59]</sup> when, in 1989, they cultured hepatocytes between two layers of collagen. This method was developed due to the difficulty of hepatocytes survival under the conventional 2D culture methods. Nowadays, sandwich cultures are composed of hepatocytes grown between two layers of ECM as collagen, fibronectin, or Matrigel, and several procedures have been described to culture hepatocytes from humans or other species.<sup>[60]</sup> The liver's metabolic functions result from the polarized epithelium of hepatocytes, which, in turn, depend on interactions between the hepatocyte cytoskeleton, cell–cell contacts, and the ECM.<sup>[61]</sup> This approach also established a long-term culture of rat hippocampal neurons at low density, significantly contributing to neuroscience.<sup>[62]</sup> Kaneko and Sankai<sup>[62a]</sup> developed a method for long-term ( $> 2$  months) primary culture of rat hippocampal neurons in a serum-free medium at low density without a glial feeder layer. The neurons were plated on a 3D nanofibrous hydrogel (PuraMatrix) and sandwiched under a coverslip to reproduce the *in vivo* environment. **Figure 3A,B** shows a color 3D image of the surface roughness of PuraMatrix as well as the respective high contrast 3D image of primary neurons (dark color) cultivated on that surface, respectively. **Figure 3C,D** shows fluorescence images of living cells of 3D growth of neurites at the rough surface of 25% PuraMatrix, coverslipped 3 h after plating (C), or not (D). This new method promoted neuronal survival and neurite extension, contributing to a better simulation of the interactions and network struc-

ture *in vivo*, making it a viable option for drug screening and toxicity.

These strategies are essential in overcoming some of the limitations of conventional 2D cell culture, providing this method with functionalities that bring artificial conditions closer to real ones. However, they are pseudo-3D microenvironments that do not accurately translate the 3D microenvironment and, as such, the complex properties and architecture of *in vivo* tissues. Therefore, in an attempt to establish more realistic biomechanical and biochemical microenvironments and avoid costly failures in the late stages of drug development, the scientific community has favored the development of 3D cell culture methods<sup>[63]</sup> to enhance predictability in drug discovery.

## 2.2. 3D Cell Culture Methods

3D cell culture creates an artificial environment that allows cells to grow and interact with each other and the surrounding space in the three dimensions. As a result, 3D cell culture has increased interest in cell biology research for drug development and screening due to the improved simulations of *in vivo* microenvironment and its complex interactions.<sup>[63,64]</sup>

To create accurate *in vivo* spatiotemporal conditions for cell development and the mechanically active microenvironment, several 3D cell culture techniques have been established. Those

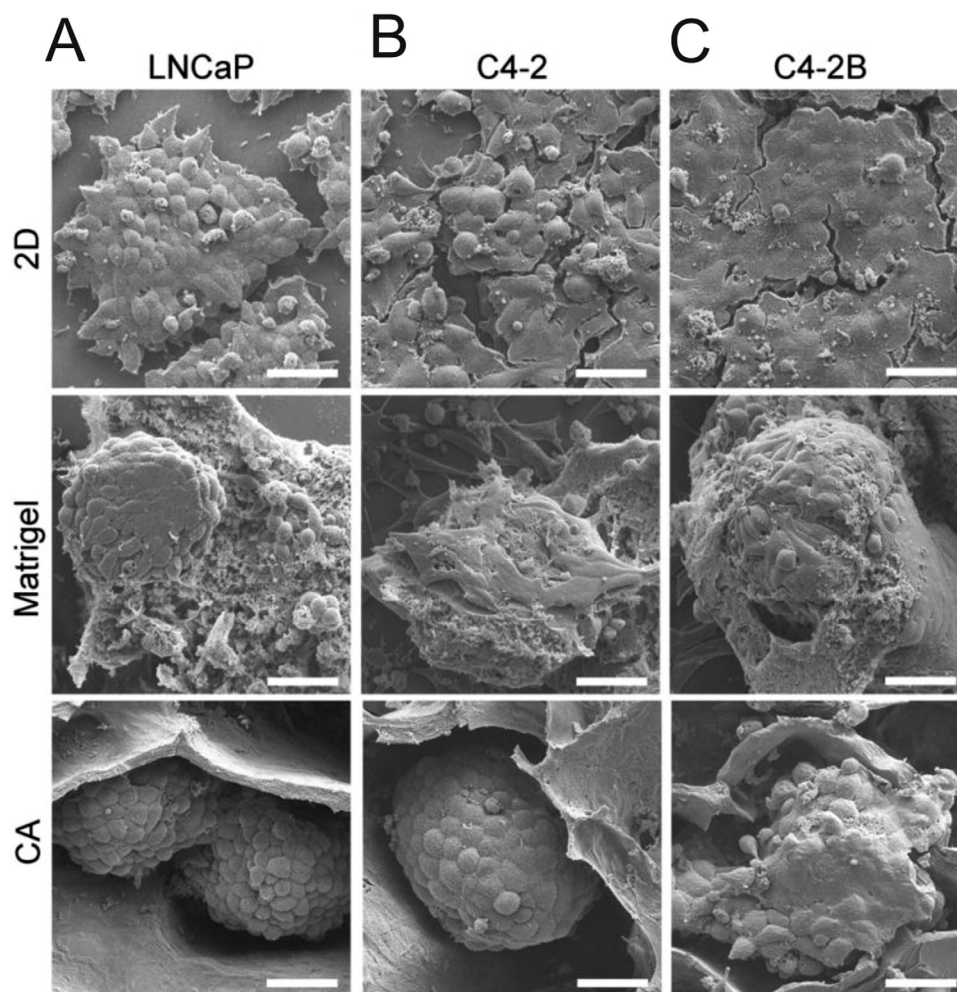


**Figure 4.** Scanning electron microscopy (SEM) images of A) LNCaP, B) C4-2, and C) C4-2B human PCa cells grown on 2D culture plates, Matrigel matrix, and CA scaffolds (bottom) for 15 days. Scale bars are 40  $\mu\text{m}$ . Reproduced with permission.<sup>[69]</sup> Copyright 2012, Wiley-VCH GmbH.

strategies include 3D nonscaffold-based cellular aggregates, hydrogel-based cell cultures, and insert scaffold-based cellular cultures.<sup>[44b,63,65]</sup> Different biodegradable polymers have been explored as supporting matrices (scaffolds) for vascularized tissue engineering, including poly(DL-lactic-co-glycolide) (PLGA), poly(glycerol sebacate) (PGS), silk fibroin (SF), and poly(1,3-diamino-2-hydroxypropane-co-polyol sebacate) (APS).<sup>[66]</sup> Cells can also be encapsulated and immobilized into hydrogels that act as scaffolding materials.<sup>[67]</sup> Using hydrogels as scaffolding materials allows the encapsulation of cells into the hydrogel while permitting diffusive permeability to oxygen and the mass transport of nutrients to encapsulated cells.<sup>[67,68]</sup> Native ECM proteins have been employed as hydrogel scaffolding basis, including fibrin, hyaluronic acid, collagen, fibronectin, agarose, Matrigel, and poly(ethylene glycol) diacrylate (PEGDA).<sup>[67]</sup> Gel-free 3D cell culture is another suitable approach to culture cells that proliferate with low ECM ratios and high cell densities, such as multicellular tumor spheroids. Another consideration must be deliberated is that cell morphology is highly dependent on the culture environment, even among different 3D cell culture techniques. Florczyk and co-workers<sup>[69]</sup> demonstrated these differences by culturing

human prostate cancer (PCa) cells (LNCaP, C4-2, and C4-2B) in 2D, seeded on Matrigel matrix and 3D porous chitosan–alginate (CA) scaffolds for 15 d (**Figure 4**). Cells grown in 2D revealed to form flat layers. In the case of the Matrigel, samples had a linear and elongated morphology and created dense, thick cell sheets in some regions. Finally, the CA scaffold samples demonstrated tumor spheroid formation within the scaffold pores.

ECM's fundamental role in regulating cell-to-cell interactions, cell differentiation, and growth<sup>[70]</sup> requires understanding how its composition and structure influence biological mechanisms, as these influence the therapeutic effects of drugs. Cultured cells in a 3D microenvironment with ECM components were revealed not only to induce the expression of genes not expressed in 2D cultures<sup>[71]</sup> but also to synthesize the ECM components themselves, as happens in vivo regeneration.<sup>[70,72]</sup> Advances in this area have been followed by the development of biomaterials that better resemble ECM and enhance cell culture efficiency and cellular functions. Some of these biomaterials include hydrogels,<sup>[73]</sup> decellularized native tissue,<sup>[74]</sup> ultralow attachment surface,<sup>[75]</sup> and solid scaffolds.<sup>[73c,76]</sup> Thus, 3D cell culture has

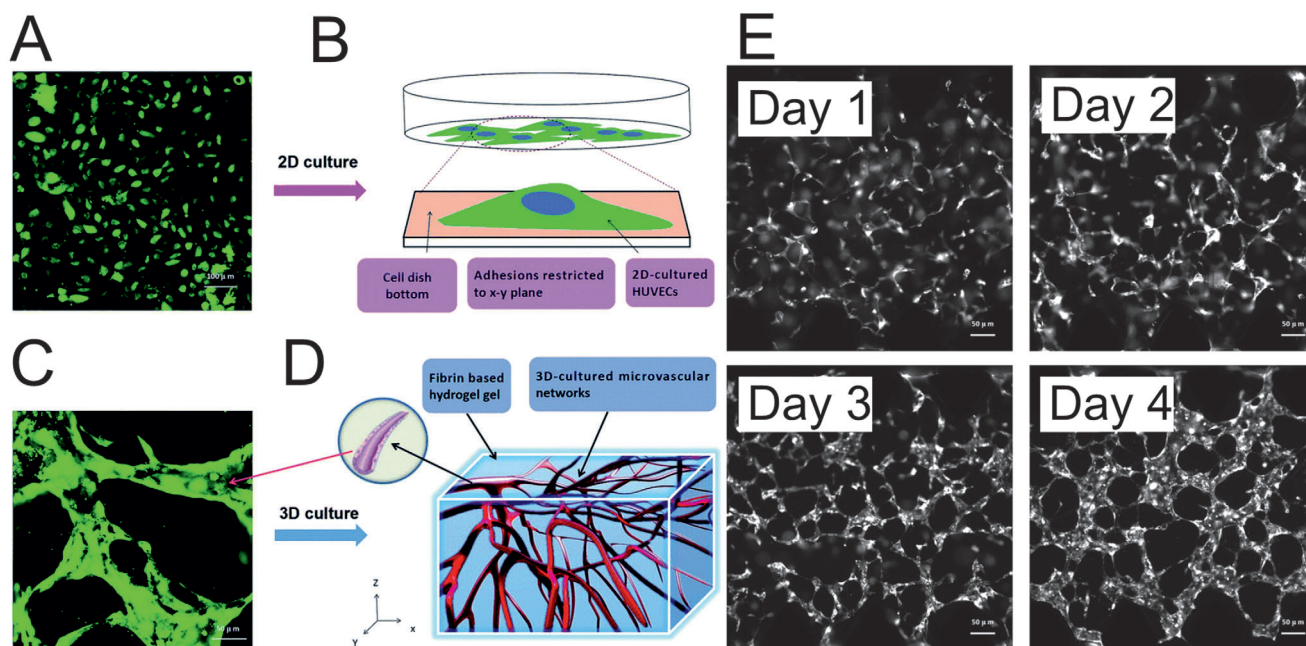


**Figure 5.** A) Confocal microscopy image of 2D cultured HUVECs. B) Schematic representation of 2D cultured HUEVECs, attached to a cell dish. C) Confocal microscopy image of the 3D microvascular network. D) Schematic representation of 3D cultured HUEVECs, where the microvessels were generated in a fibrin-based scaffold; E) Development progress of microvascular networks was monitored by a camera in a confocal microscope. Adapted with permission.<sup>[80]</sup> Copyright 2017, The Royal Society of Chemistry.

been used in regenerative medicine,<sup>[77]</sup> disease modeling,<sup>[78]</sup> and drug screening.<sup>[79]</sup>

In a work related to the toxicological effect of ambient fine particulate matter (FPM) on microvascular networks, the 2D culture of human umbilical vein endothelial cells (HUVECs) was compared to the 3D cell culture counterparts.<sup>[80]</sup> In conventional 2D cell culture, the HUVECs cells adhered and spread on the flat plastic surface, forming unnatural cell attachments that do not allow the representation of essential cellular functions of tissues (Figure 5A,B). Fibrin gel was used to generate scaffolds for the organotypic culture in the 3D model, where the HUVECs grew and formed capillary-like microtissues with lumens (Figure 5C,D), providing a model that mimics the morphology of microvessels and simulates some physiological functions of human blood vessels.<sup>[80]</sup> Figure 5E shows the development progress of microvascular networks monitored by a camera in a confocal microscope over 4 d. On days 1 and 2, the HUVECs migrated to form cell–cell adhesions and alignments. Then, on day 3, HUVECs gradually developed lumens along with cell proliferation, culminating in microvascular networks formed on day 4.

The access to functional differences of 2D monolayers compared to 3D microenvironments has been carried out, mainly in cancer research. Hickman et al.<sup>[81]</sup> reviewed human cancer models that aim to reproduce the heterogeneity and complexity of human cancer in situ. Imamura et al.<sup>[82]</sup> demonstrated that some breast cell lines (namely, BT-549, BT-474, and T-47D) formed dense 3D multicellular spheroids (MCSs), and those spheroids decreased the sensitivity to the chemotherapeutic drugs doxorubicin (DXR) and paclitaxel (PTX) when compared to 2D cultured cells. The results revealed that chemoresistance might result from MCSs hypoxia, associated with an in-

creased G0 phase cell population and/or downregulation of proapoptotic molecules.<sup>[82]</sup> Recently, similar results were observed in head and neck squamous cell carcinoma (HNSCC) cell lines (namely, LK0902, LK0917, and LK1108), revealing that 3D cultured cells are less sensitive to cisplatin (DDP) when compared to the 2D counterparts.<sup>[83]</sup> In the same study, the expression of CSC-associated transcription factors (as NANOG and SOX2) increased in all the studied cell lines cultured in 3D. No specific pattern was found between epithelial–mesenchymal transition (EMT)-associated protein expression and drug response, but the increase in EMT protein expression led to increased migration of tumor cells growing in spheroids.<sup>[83]</sup>

Although this method brings clear advantages with respect to conventional methods, there are some challenges and limitations in the widespread use of 3D models. It is pointed to a low reproducibility and an increased difficulty in data interpretation.<sup>[84]</sup> Despite all the advances, it is a growing area, still lacking an intensive characterization and validation of models for the different pathologies, leaving some biological properties (such as gene expression, growth kinetics, and signaling cascades) with no comprehensive understanding.<sup>[81]</sup> Some other limitations are related to restricted cell observation and extraction for further analyses, difficulties in obtaining some 3D systems types, and the time and money-consuming process implicated in maintaining the cultures.<sup>[85]</sup> Furthermore, some 3D culture approaches do not address the static nature of 2D culture since it also requires regular media changes to remove cell wastes and nutrient restoration. These extra steps are associated with an increased risk of experimental errors and sample contamination. **Table 1** summarizes the advantages and challenges of 2D and 3D cell culture methods.



**Table 1.** Summary of the advantages and challenges of 2D and 3D cell culture methods.

Cell culture method	Advantages	Challenges
2D	<p>Long-term culture, high reproducibility, simple and easy to interpret</p> <p>Homogeneous growth and proliferation of cells</p> <p>Relatively low-cost maintenance</p> <p>Well-established methods with commercially available media</p> <p>Homogeneous growth and proliferation of cells</p>	<p>Inability to simulate <i>the in vivo</i> microenvironment and the cellular architecture</p> <p>The morphology of tissues or organs is changed</p> <p>Loss of multiple phenotypes and polarity expression</p> <p>Changes in the proliferation, cell-cell connections, cell-matrix connections, migration, survival, adhesion, and differentiation</p> <p>Do not allow the simulation of oxygen or nutrient gradients that occur naturally <i>in vivo</i></p>
3D	<p>Improved simulations of <i>in vivo</i> microenvironment and its complex interactions</p> <p>The morphology of tissues or organs is preserved</p> <p>Polarity differences and multiple phenotypes</p> <p>Accurate <i>in vivo</i> spatiotemporal conditions for cell development and the mechanically active microenvironment</p> <p>Allow the simulation of oxygen or nutrient gradients that occur naturally <i>in vivo</i></p>	<p>Long-term culture is difficult, with lower reproducibility, and more significant difficulties in interpreting results</p> <p>Still lacking an intensive characterization and validation of models for the different pathologies</p> <p>Money-consuming process and time-consuming</p> <p>Restricted cell observation</p>

### 2.3. Final Remarks on Conventional Cell Culture Methods

Notwithstanding the limitations of both 2D and 3D cell cultures, their importance as essential laboratory approaches to pharmacology and therapeutic research must be highlighted again. The challenges in each technique have also encouraged to development of solutions that can increasingly provide more complex and accurate pharmacological profiles.

Furthermore, the parallel advances in biomaterials science and microengineering allowed the researchers to refine some approaches by enabling the regulation of *in vitro* microstructure and mechanical properties, aiming to mimic the biochemical functions of living organisms.<sup>[86]</sup> Integrating knowledge from these areas resulted in microfluidic cell culture systems as a new dimension for understanding cell behavior in drug screening.

## 3. The Convergence between Cell Culture and Microfluidic Platforms

### 3.1. Overview of Manufacturing Processes and Materials

The use of microfluidic devices in life science research has increased mainly upon the invention of soft lithography<sup>[87]</sup> and large-scale microfluidic integration.<sup>[88]</sup> These achievements allowed the establishment of a more straightforward, versatile, and sophisticated method of producing devices, enabling the adjustment of prototypes to the complexity of biological organisms. The fabrication of disposable microfluidic devices includes several techniques, such as photolithography, soft lithography, hot embossing, *in situ* construction, laser ablation, injection molding, micromachining, wet etching, and reactive ion etching.<sup>[89]</sup> Soft lithography is a set of techniques for fabricating micro- and nanostructures based on printing, molding, and embossing with an elastomeric stamp,<sup>[90]</sup> and it is the most popular technique for fabricating microfluidic devices. This technique allows the development of structures with sizes from  $\mu\text{m}$  to less than 100 nm. The resolution limit is determined by the balance of the wetting, van der Waals, and kinetic factors.<sup>[90]</sup> Detailed information about

soft lithography fabrication methods, materials, and the integration of microfluidic systems with physical micro/nanostructures fabricated by soft lithography is reviewed in ref. [91].

Polydimethylsiloxane (PDMS) is the most used material in this technique due to its functional and physical properties. The fabrication of PDMS microfluidic devices consists of two main steps: the fabrication of the stamp by a photolithography process and the molding (Figure 6).<sup>[89b]</sup> This elastomer presents practical advantages, including fast processing, low cost, reusability of the masters (e.g., resin SU-8), and easy sealing and bonding to different substrates.<sup>[89b]</sup> In addition, PDMS is an excellent material for cell-based assays as it is gas permeable, presents favorable biochemical reliability, is nontoxic, presents appropriate optical properties (such as optical transparency and low autofluorescence), is autoclavable, and allows the easy integration of fluidics interconnects (as valves and pumps to control the fluid flow).<sup>[89b]</sup>

The majority of currently used microfluidic devices in research and development are manufactured by soft lithography and PDMS.<sup>[92]</sup> Although it is a relatively straightforward process, the use of PDMS microfluidic devices raises some challenges associated with the high cost of the cleanroom setup and the difficulty of mass production that hinders its commercialization.<sup>[93]</sup> Furthermore, PDMS faces challenges driving the use of PDMS-alternative materials to fabricate the devices, which will be detailed in the following sections. In addition to device manufacturing aspects, the successful convergence of microfluidics with cell culture is a complex process that requires consideration of several other operational and biological concerns. Thus, the following sections integrate knowledge concerning the effects of miniaturization, the integration of components to control cell seeding, the pump of media to cells, the transport of fluids between regions, and the control of fluid flow. All these elements must be considered individually and together when designing, using, and analyzing results from a microfluidic cell culture platform.

3D-printed microfluidic devices have been established as a viable alternative, registering a growing trend since 2014.<sup>[93]</sup> The ability to manufacture the device on a single machine makes the overall process faster, easier, and cheaper.<sup>[94]</sup> Furthermore, the

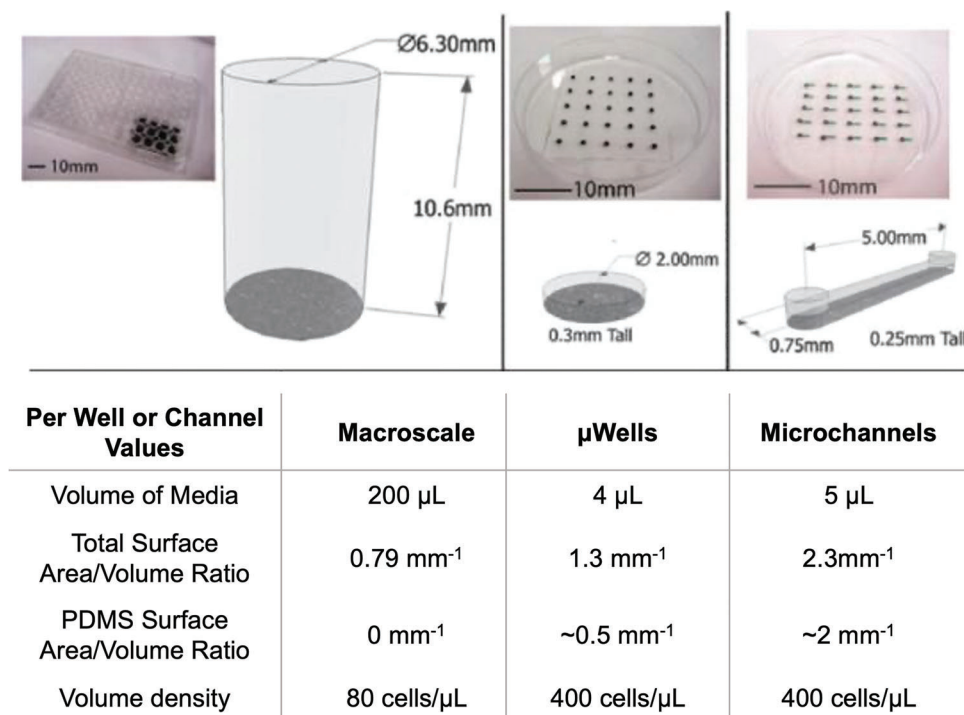


**Figure 6.** The fundamental differences between macroscale,  $\mu$ wells, and microchannels culture devices concerning the total media volume, SAV ratios, and volume densities.  $\mu$ Wells is a PDMS stencil placed on tissue culture plastic similar to microchannels. Adapted with permission.<sup>[113]</sup> Copyright 2009, Oxford University Press.

molding methods can only be used to create pseudo-3D, not truly 3D networks, because the molding material and the master structure are interlocked during the molding process.<sup>[94b]</sup> The most widely used technologies to produce 3D-printed microfluidic devices are stereolithography, inkjet 3D printing, and extrusion-based technology (for detailed information see<sup>[94a]</sup>). The scientific community has been addressing some of the 3D-printed microfluidic devices' challenges, such as printing resolution, low optical transparency, autofluorescence, surface roughness, and low gas permeability.<sup>[93–95]</sup>

### 3.2. Physical Considerations in Miniaturizing Cell Cultures

The general idea of using microengineering devices is to condense conventional chemical and biological laboratories into one device. However, scaling down standard laboratory procedures by a factor of 1000 or more implies physical changes that require a rebuild in our critical and analytical view.<sup>[96]</sup> At the micrometer scale, fundamental physical and chemical scaling effects occur since different forces become dominant. This phenomenon ensures that at the microscale, the physical parameters are very similar to those naturally occurring under physiological conditions, namely the surface area-to-volume (SAV) ratio, laminar flow, and an effective culture volume.<sup>[89a,96,97]</sup>

At the macroscale, the inertia force effect dominates the flow action. As the scale is reduced, the viscous force effect becomes dominant, leading to a small number of Reynolds and dominating the laminar flow.<sup>[98]</sup> Reynolds number (Re) is a dimensionless number defined as the ratio of inertial force to viscous

force that describes a fluid flow regime—laminar or turbulent. A laminar flow results from the channel dimensions, fluid properties, and flow velocity.<sup>[89a]</sup> This behavior is numerically indicated by  $Re < 2300$ , in which the velocity of a particle in a fluid is not a random function of time.<sup>[89a]</sup> The small dimension of microchannels results in a low Re number (e.g.,  $10 > Re > 0.001$ ),<sup>[99]</sup> making the flow regime almost always laminar with no turbulence. As a result, the dominant mass transport type changes from convection to diffusion.<sup>[98]</sup> This regime was explored, for instance, to pattern the cell culture substrate and the cell culture media and perform patterned cell deposition.<sup>[100]</sup> It introduces two different fluids flowing side by side in a stable stream with a common interface. This behavior allows for performing a set of chemical manipulations, such as solvent extraction and phase separation.<sup>[101]</sup> In the laminar flow context, diffusion can be a process with substantial influence on the movement of soluble components through the microchannels. Since diffusion is a slow process at the microscale, microchannels can create concentration gradients with complex profiles. Dertinger et al.<sup>[102]</sup> explored microfluidic networks to describe the generation of gradients with complex shapes in solution, demonstrating that gradients are maintained across a broad channel (900–2100  $\mu$ m width) over several tens of seconds. The miniaturization is accompanied by a significant increase in the SAV ratio, dominating the surface and edge effects from viscous force and surface tension on thermal transmission.<sup>[98]</sup> The enhanced SAV ratio reduces the diffusion distance and the mass and heat transfer time, decreasing the reaction times.<sup>[103]</sup> High heat-exchange efficiency allows rapid heat or cools the mixture, ensuring isothermal conditions with accurately defined residence times.<sup>[104]</sup> Detailed



information about the fundamental laws and theoretical principles underlying the operation of microfluidic devices can be found in.<sup>[96,98]</sup>

### 3.3. Implications in Miniaturizing Cell Cultures

These scaling effects in microfluidic channels are well suited to cells' biological and physical context in a living organism.<sup>[105]</sup> Thus, the small dimensions of microfluidic devices are the leading cause of direct and indirect advantages that these platforms offer to perform biological experiments compared to traditional cell cultures in well plates or Petri dishes. The main benefit microfluidic technology offers cell culture is its ability to provide personalized control over culture conditions, the fluids flow, and the chemical and physical microenvironment in vitro.<sup>[106]</sup> Microfluidic devices can create spatiotemporal gradients, and dynamic fluid flows, control the delivery of nutrients and chemical cues to cells,<sup>[1]</sup> and patterned cell culture substrates inside the device.<sup>[100]</sup> They also control cell counts and density in a specific area or volume while placing cells in complex geometries,<sup>[107]</sup> individual recovery during or after studies, and high spatial and temporal resolution monitoring. As detailed in the 3D cell culture section, this approach also allows structuring cells in 3D geometries and, thus, creating conditions even more similar to physiological ones.<sup>[108]</sup>

Furthermore, each microfluidic device can be designed for specific cell types as monoculture and can also implement the coculture of different cell lines due to the flexibility in the device design.<sup>[99]</sup> Since the microchannels scale meets the scale found in the cellular microenvironment and the ratio between cell volume and extracellular fluid volume is more significant than one, a more similar cellular context is ensured.<sup>[109]</sup> In turn, miniaturization reduces the volume of reagents, samples, and cells used per assay, which is advantageous for waste reduction<sup>[110]</sup> but requires the consideration of other effects. It is also an alternative to limited resources and costly growth factors or inhibitors, reducing the overall cost of cell culture studies compared to 96-well plates.<sup>[111]</sup> The cell population in the microfluidic strategy comprises a few hundred cells (or even a single cell<sup>[112]</sup>), highly contrasting with the  $10^4$ – $10^7$  cells of macroscopic cell cultures.<sup>[97]</sup> This reduction in cell number increases the spatial and temporal resolution of the assays since it allows the capture of changes in the behavior of cells to the individual level that otherwise would become unnoticed in a larger group of cells.<sup>[97]</sup> Ren et al.<sup>[112]</sup> reported a microfluidic device composed of multiconstriction channels able to differentiate a human breast cancer cell line (MDA-MB-231) and a non-tumorigenic human breast cell line (MCF-10A). The work was based on the principle that non-neoplastic and neoplastic cells present different velocity profiles due to the lower membrane stiffness and cytoskeleton of cancer cells.<sup>[112]</sup>

As previously referred, the reduction in the volume of reagents has clear advantages; however, it is also necessary to consider the differences and limitations of the change in volumetry. The miniaturization increases the susceptibility to liquid evaporations, which, in turn, results in a significant increase in osmolality. For instance, while in macroscale cultures, the evaporative loss of 1 mL corresponds to a 0.5% shift in osmolality,

in microfluidic culture, the osmolality shift deviates to a 33% increase.<sup>[113]</sup> An increase in osmolality is translated into changes in cellular growth, signaling, gene expression, metabolism, and cellular growth.<sup>[114]</sup> Evaporation losses are particularly challenging when using PDMS-based microfluidic devices since it is a vapor-permeable material. Heo et al.<sup>[114]</sup> characterized the problem using PDMS membranes with varying thicknesses, concluding that the evaporation-mediated osmolality shifts are faster with thin PDMS membranes. Also, humidified and non-humidified cell culture incubators prevented mouse embryo and human endothelial cell growth and development. The authors proposed a PDMS-parylene-PDMS membrane, which has proven effective in preventing evaporation, resulting in the development of single-cell embryos to the blastocyst stage and culture of human endothelial cells under a non-humidified environment.<sup>[114]</sup>

Additionally, the volume density of microfluidics-based cell culture significantly differs from other cultures. Conventional cell culture techniques present reduced volume density, meaning that large media volumes cover few cells compared to microfluidic devices. It is estimated that for the same cell surface density, a slightly large microchannel (with dimensions of 750  $\mu$ m wide, 5 mm long, and 250  $\mu$ m tall) presents a volume density 2 to 4 times higher than the macroscopic six-well plates while using 250 times fewer cells, and 500–1000 times fewer media and costly reagents.<sup>[115]</sup> Higher volume density means reducing the total amount of the media components available for each cell and a higher rate of accumulation of waste products. Even though lowering the available medium per cell possibly affects cell behavior, those effects on cellular functions are unclear.<sup>[115]</sup> Paguirigan and Beebe<sup>[113]</sup> analyzed the effects of media supplementation (varying serum and glucose concentrations) and the effects of volume density on cell proliferation in microchannel and macroscale cultures. For this, the authors used three culture devices (macroscale,  $\mu$ Wells, and microchannels) to identify how the variation of different characteristics, such as small volume, volume density differences, and interactions with PDMS, impact cell behavior. The fundamental differences between macro and microculture devices are represented in Figure 6. The results revealed a significant proliferation reduction in microchannel cultures 2.5 and 5 times compared to the corresponding density in macroscale cultures. However, in contrast to macroscale cultures, microchannel culture did not show a significant variation in the proliferation rate in the different volume density variations. The results suggest volume density is not a predominating factor in regulating proliferation rates. Those effects can be partially related to the continuous nutrient supply and waste removal in microfluidic systems.<sup>[113]</sup>

In addition to scaling out effects, the manufacturing methods, the fabrication materials, integrated components, and the geometry of the cell culture sites also highly differentiate the microfluidic cell cultures from other cell culture techniques. Therefore, the design of microfluidics-based cell culture devices must consider the effect of those factors singularly and combined since small changes in the approaches or features of the devices can be translated into different cellular responses. Kim et al.<sup>[68]</sup> were pioneers in the systematic discussion of the design principles of microfluidic perfusion culture systems and the practical issues that the operation of these systems raises in biomedical applications.

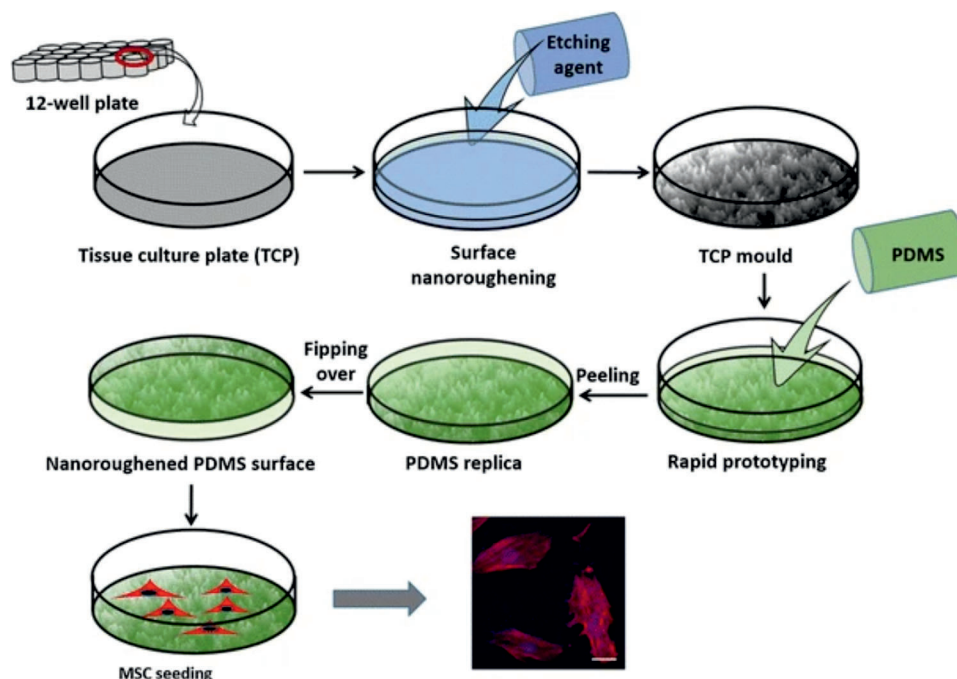


**Figure 7.** Schematic representation of nano roughened PDMS substrate fabrication using acetone etched PS mold. Reproduced with permission.<sup>[120]</sup> Copyright 2018, Springer Nature.

### 3.4. Operational Considerations in Miniaturizing Cell Cultures

In microfluidics-based cell culture platforms, cells can be cultured in 2D monolayer or 3D configurations. In general, the same advantages of 3D cell culture at the macroscopic level (see Section 2.2) can be pointed out at the microscopic level; a more reliable representation of physiological conditions results in a better prediction of physiological behaviors and associated cellular responses. First, most mammalian cells need solid substrates or scaffolds to proliferate.<sup>[116]</sup> Thus, microfluidics-based cell culture platforms must provide suitable biochemical and biomechanical support. Different materials can be incorporated into microfluidic microchambers to act as cell substrates in 2D perfusion cultures.

As previously mentioned, PDMS is the most used material for the fabrication of microfluidic devices. Despite the indisputable advantages of PDMS for microfluidics-based cell culture development, this elastomer raises some technical issues that should be considered. The organic methyl groups in its chemical structure make this polymer hydrophobic, leading to poor wettability, which results in poor cell adhesion and dissociation of cell aggregates or islands on the PDMS surface.<sup>[117]</sup> Several methods have been employed to modify the physicochemical properties of PDMS surfaces. Those include gas phase processing methods (plasma treatment, chemical vapor deposition (CVD), ultraviolet (UV) irradiation, and metal oxide coating) and wet chemical methods (layer-by-layer (LBL) deposition, silanization, dynamic surface modification, and sol-gel coating).<sup>[118]</sup> In addition, the PDMS coating with ECM proteins such as fibronectin, collagen, laminin, and/or gelatin has been used to provide natural moiety for cell anchoring and survival.<sup>[119]</sup>

Furthermore, physical modifications on the PDMS surface, such as surface roughness modification, can also improve cellular adhesion. Recently, Xue et al.<sup>[120]</sup> developed a method to precisely control the PDMS nanoroughness using an etched polystyrene (PS) culture plate by varying the etching time and the etchant concentration. The process is based on two main steps: 1) Chemical etching process, using acetone, of PS stencil of tissue culture plates; and 2) PDMS prepolymer cast against the PS master (**Figure 7**). The area of cell spreading increase was positively correlated with both etchant concentration and etching time, implying that nanoroughened PDMS surface may enhance surface biocompatibility and facilitate cell spreading. Furthermore, the results revealed an improvement in the adhesion and proliferation of MSC, standing out as an effective alternative to engineering the cell-PDMS interfaces for in vitro cell studies.<sup>[120]</sup>

Another disadvantage is the adsorption of compounds present in the culture medium to PDMS, which is particularly significant with small hydrophobic molecules such as drugs.<sup>[121]</sup> Toepke and Beebe<sup>[122]</sup> qualitatively verified the absorbance of small hydrophobic molecules (Nile red and quinine) into PDMS by a fluorescence assay. Further, channel reduction implies an increased SAV ratio, exacerbating the problem. Drug adsorption reduces the available drug, whose effect may be especially significant in assays that aim to assess changes in cellular behavior and the effects caused by certain medicines since their adequate availability to cells is altered. Meer et al.<sup>[123]</sup> quantitatively compared the absorption of four cardiac drugs (verapamil, bepridil, Bay K 8644, and nifedipine) in which there is clinical interest in accurately determining their toxic threshold. The results revealed that the presence of PDMS significantly changed the concentration of all free drugs. Still, no clear correlation

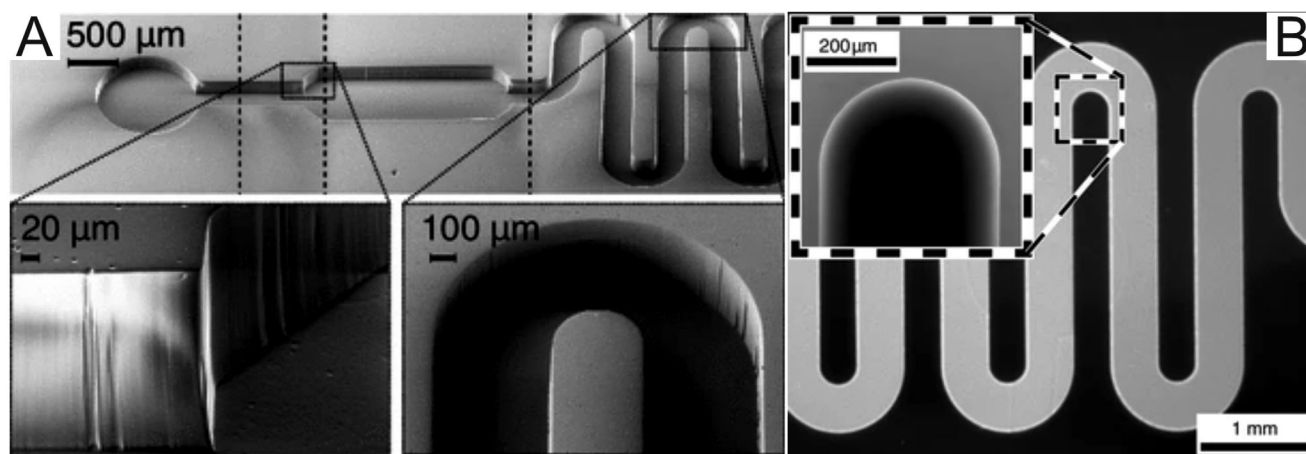


**Figure 8.** A) SEM images of the microchannel fabricated by lithography and respective close-ups at the bottom. B) Fluorescence images of the microchannels filled with Rhodamine B solution 69 h after injection. No leakage could be detected, indicating a leak-free bond interface. Adapted with permission.<sup>[129]</sup> Copyright 2014, Springer Nature.

was found between the compounds' absorption and molecular weight or log  $P$  (which measures how hydrophobic/hydrophilic a molecule is). Contrasting to the previous studies of Wang et al.,<sup>[121b]</sup> it was concluded that hydrophobicity and molecular weight are not, at least, the only parameters that determine the binding of small molecules to PDMS. Nevertheless, a correlation between topological polar surface area and absorption of small hydrophobic molecules was found.<sup>[123]</sup> Therefore, several PDMS surface modification approaches have been proposed to reduce nonspecific adsorption and absorption. Besides those mentioned above, they include poly(ethylene glycol) (PEG) addition into PDMS prepolymer before curing,<sup>[124]</sup> PDMS surface silanization with (3-aminopropyl)triethoxy silane (APTES), and glutaraldehyde (GA),<sup>[125]</sup> pluronic addition into uncured PDMS,<sup>[126]</sup> PDMS modification with titanium dioxide and derivatization with oligoethyleneoxide,<sup>[121a]</sup> parylene coatings,<sup>[127]</sup> or the use of commercially available CellBinder,<sup>[123]</sup> among others.

Moreover, alternative materials have been developed towards increasingly advanced mimetic materials for cell culture to overcome the previously mentioned limitations. The choice and development of new materials must consider, in the first instance, the advantages of replacing the PDMS material in device fabrication and how the new material improves interaction with cells and the reproduction of a more capable mimetic environment. Thermoplastics or UV-curable thermosets are currently viable alternatives to PDMS prototyping. Although thermoplastics (such as PS and cyclic olefin copolymers) are widely used in commercially available devices, their prototyping relies on expensive machines and tools, time-consuming surface modifications, and complicated bonding of device layers.<sup>[128]</sup> Carlborg et al.<sup>[128]</sup> developed a novel polymer platform of UV-curable off-stoichiometric thiol-ene (OSTE) polymers, designed explicitly for microfluidics and lab-on-a-chip, with similar mechanical and chemical properties as PDMS. The OSTE polymers were cast and rapidly UV-cured (<30 s) on standard silicon/SU-8 molds. Pardon et al.<sup>[129]</sup> developed an innovative method based on direct photolithographic patterning of a new OSTE polymer. Based on mold-free prototyping, this technology improves the original idea of Carborg et al.,<sup>[128]</sup> since it is fast (< 1 h) and offers more ro-

bust covalent surface modifications and bonding.<sup>[129]</sup> Before the platform was sealed, SEM images revealed an excellent pattern fidelity, characterized by microchannels 400  $\mu\text{m}$  wide and 200  $\mu\text{m}$  high (Figure 8A). To investigate the bond quality, the authors incubated the chip with rhodamine B over 69 h. The fluorescence imaging revealed a good bonding quality since no creeping of the fluorescent dye at the bond interface or diffusion inside the polymer was observed (Figure 8B).<sup>[129]</sup>

Furthermore, PS substrates were used to evaluate and quantify morphological changes of MSCs,<sup>[130]</sup> while glass substrates were used to culture human lung carcinoma cells (A549).<sup>[131]</sup> Comprehensive information about the considerations and properties of these alternative materials to PDMS is presented in ref. [132].

Another consideration that should be considered is the process that mediates the placement of a cell suspension in a cell culture chamber. The cell seeding process is also a crucial step that dictates cell cultures' viability. Syringe-controlled cell loading is the most widely used approach; nevertheless, it does not allow precise control over the loading process or the positioning of cells in a specific location. Gravity flow can be employed to achieve a more uniform cell distribution.<sup>[133]</sup> Typically, a static incubation period follows the cell seeding process to allow cell attachment. This incubation period varies according to cell type, cell seed culture medium, cell-substrate properties, and cell density.<sup>[68]</sup> A uniform cell loading and distribution in the chamber is a request in some cytotoxicity screening assays, and small perturbations to fluid flow can disturb cell distribution and induce stress to cell cultures. To address these problems, Wang et al.<sup>[134]</sup> designed a platform where the channels for seeding are orthogonal to the ones used to input drugs. They also included several U-shape micro cell sieves within each culture chamber to create low flow velocity regions and uniform distribution of small seed populations of cells ( $\approx 10$  cells per sieve). Upon appropriate cell immobilization, perfusion ensures media changes and cell culture maintenance. The perfusion system can be categorized as recirculating (the culture media recirculates in the perfusion culture) or non-recirculating (culture media is wasted after culture perfusion).<sup>[68]</sup> Thus, microfluidic-based cell cultures require proper adjustments on time intervals between media changes

since they differ from macroscopic cultures due to higher culture SAV ratios. As mentioned, some microfluidic systems applications work as continuous perfusion with media components. In these cases, appropriate perfusion rates are critical to be determined instead of time intervals. Based on geometric arguments and time scales comparison, Young and Bebee<sup>[135]</sup> introduced the concepts of effective culture time (ECT) and critical perfusion rate (CPR) that provide a guide for designing experiments and microfluidic devices.

Another crucial issue in cell culture in microfluidic devices is the selection of the appropriate technique to deliver and pump media to the cells, transport fluids between the regions of microfluidic devices, and control the fluid flow. Byun et al.<sup>[136]</sup> reviewed different passive and active pumping techniques used to perform perfusion cell culture in microfluidic platforms, covering their flow generation principle, strengths, and weaknesses. In addition, a comparison was carried out between pump characteristics for cell culture and manipulation. Those pumping techniques include gravity-driven flow, surface tension-driven flow, osmosis-driven flow, syringe and gas pressure pumps, peristaltic pumps, electrokinetic and electroosmotic pumps, and centrifugal pumping, among others.<sup>[136]</sup> Microfluidic assembly employs pumps that are either on-chip (built directly on the chip) or off-chip (externally connected to the device). Off-chip pumps are typically used in laboratory conditions; syringe pumps are the most commonly used pump in laboratory microfluidics. Syringe pumps are active mechanical pumps that employ a piston to generate positive pressure to push liquids through a conduit, enabling the delivery of constant flow rates.<sup>[136]</sup> These pumps are classified as closed systems since they cannot drive recirculating flow, have the limitation of only pumping the fixed volume of liquid enclosed in syringes, and are relatively high priced.<sup>[136,137]</sup> Peristaltic pumps are also active pumps based on the press of a flexible conduit to displace the liquid inside the conduit and can be assembled in an opened fluidic circuit (the main fluid reservoir can be refilled) or in a closed fluidic format (liquids are recirculated).<sup>[136]</sup>

Several types of on-chip peristaltic pumps have been developed in recent years, allowing precise control of small liquid volumes. For instance, Devaraju and Unger<sup>[138]</sup> created an on-chip valve based on a post-modification of a multilayer soft lithography fabrication process. By using close valves, static gain valves were fabricated that allowed the control of a higher pressure by a lower pressure, which resulted in fully cascable fluidic logic circuits.<sup>[138]</sup> However, this class of peristaltic pumps still requires complex fabrication procedures and limits the geometry of microfluidic devices. To reduce the complexity and the cost of device designs and fabrication, Zhang et al.<sup>[139]</sup> obtained a valve-less micropump with single-layer lithography, where bearings squeeze the microchannels. In this approach, a PDMS chip was designed with a linear microchannel, and a cam (or bearing) was placed on top of it (Figure 9A-i). When the cam squeezes the microchannel, the liquid is pumped from the inlet to the outlet, and the chip slides from left to right (Figure 9A-ii). As the spring is released, a backflow occurs due to the PDMS deformation recovery, and the liquid is pumped through the microchannels from one port to the other (Figure 9A-iii). This novel peristaltic pumping mechanism enables the precise control of the flow at the range of 1 to 500 nL s<sup>-1</sup>, holding the potential of being inte-

grated into several microfluidic applications with single and multiphase complex flows.<sup>[139]</sup> Commercially available off-chip valve peristaltic pumps are also a good solution, but they are a relatively expensive choice. Recently, Behrens et al.<sup>[137]</sup> proposed a low-cost (<\$120) peristaltic pump that combined 3D-printed components and standard hardware. The pump was also designed to be open-source and reprogrammable, allowing a functional adaptation to operator-defined requirements and programmable flow profiles suited for various applications (Figure 9B-i).<sup>[137]</sup> Fluids' motion through the tubing is a result of cyclical compression of the tubing by a rotor (Figure 9B-ii), and the respective pump rate is dependent on the tubing diameter and the rotation speed of the pump (Figure 9B-iii).<sup>[137]</sup> Also, in contrast to syringe pumps, this peristaltic pump allows driving recirculating flow in a closed system.

Understanding the physical and biological processes that follow miniaturization and the development and integration of functional components have driven the rapid growth of microfluidics-based drug screening platforms in recent years. Currently, they are already established as a low-cost, reproducible, and fast alternative, allowing high throughput drug screening and playing an essential role in reducing animal testing and associated ethical issues.

## 4. Recent Advances in Microfluidics-Based Cell Culture Devices for Drug Screening and Cell Therapies

Microfluidic drug screening platforms can rely on different analysis approaches, which can be focused on drug activity screening, drug cytotoxicity, or, for instance, the combination of multiple drug screening. This section will highlight recent advances in microfluidics platforms for 2D and 3D cell-based drug screening. Relevant devices in the field will be presented, namely gradient-based microfluidics, droplet-based microfluidics, printed-based microfluidics, digital-based microfluidics, SlipChip, and paper-based microfluidics.

### 4.1. Concentration Gradient-Based Microfluidics

Concentration gradients play an active and relevant role in cell biology, being responsible for various cellular behaviors such as cell growth and differentiation,<sup>[140]</sup> wound healing,<sup>[141]</sup> chemotaxis,<sup>[142]</sup> inflammation,<sup>[143]</sup> signaling,<sup>[144]</sup> and cancer metastasis.<sup>[145]</sup> Thus, one of the greatest ambitions in life sciences is related to the ability to recreate physiologically relevant environments, bringing in vitro cell models closer to the organization found in vivo. Considering the microfluidics advantages presented in previous sections (such as the low Reynolds number, fast and cost-effective technology, and the possibility of observing cellular processes in real-time), microfluidic concentration gradient generators (CGG) are excellent candidates to recreate those gradients, even allowing the control of events in time and space. Furthermore, these devices can also generate a concentration range of an input drug or compound, allowing to optimize of drug discovery processes in a faster and more accurate way, ensured by the possibility of cultivating different cell



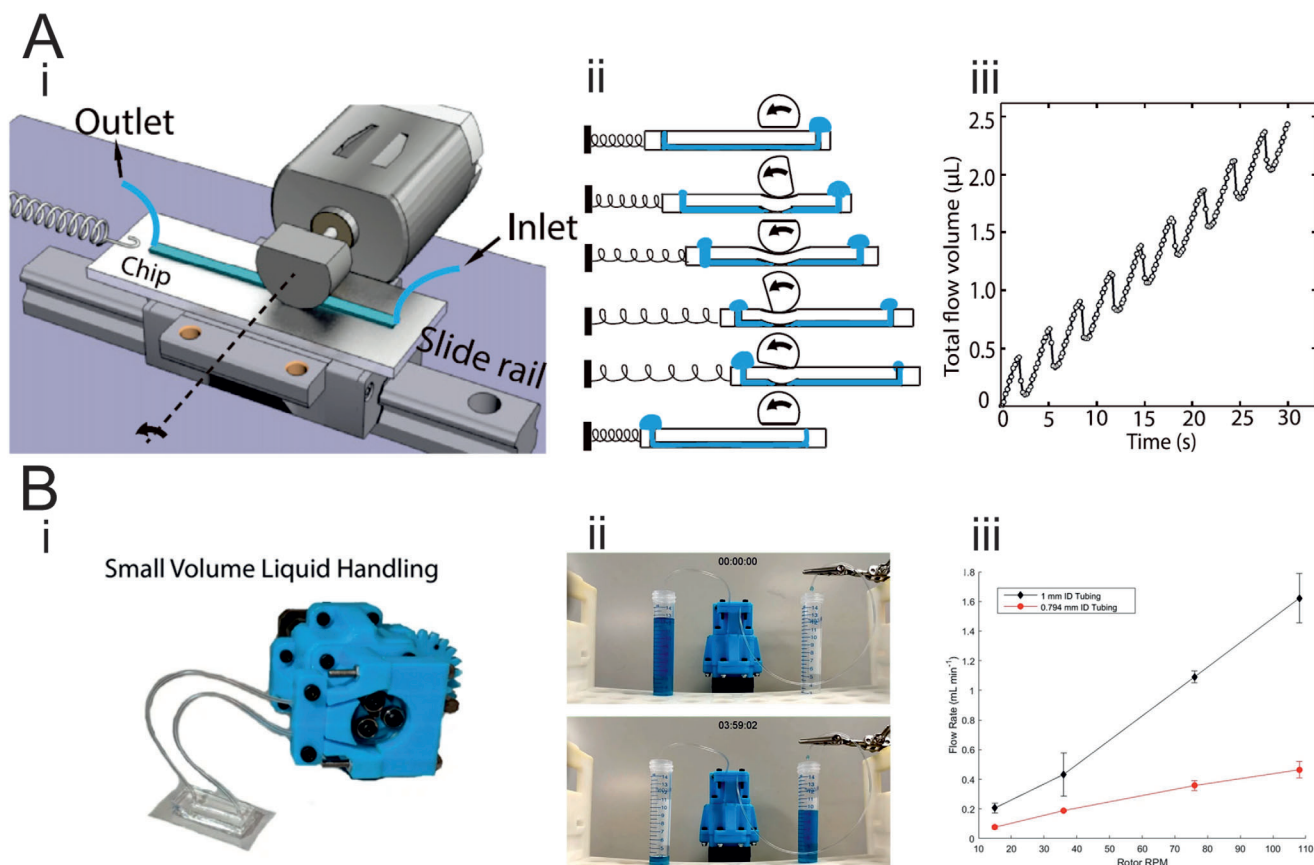


**Figure 9.** Comparison between two proposed peristaltic pump mechanisms. A-i) Microfluidic chip containing a linear channel placed on a slide rail squeezed by a rotating cam on top; ii) Schematic showing how flow is pumped during each cycle; iii) Total flow volume accumulated with time.<sup>[139]</sup> B-i) Open-source, 3D-printed programmable peristaltic pump that can be used for precision low-volume liquid handling. The pump is assembled with a combination of 3D-printed parts and commonly available hardware and is programmable via an Arduino microcontroller; ii) The pump uses the peristaltic motion of rotating ball bearings with silicone tubing to transfer fluid; iii) Flow rate controlled by varying the rotation speed of the pump, or by varying the diameter of the tubing. Adapted with permission and under the terms of the CC-BY-4.0 license,<sup>[137,139]</sup> Copyright 2015 and 2020, the Authors. Published by AIP Publishing and Springer Nature, respectively.

lines and treating them with a range of drug concentrations (free or encapsulated form) in a single regimen assembly.<sup>[146]</sup> According to their gradient-generating principles, microfluidic CGG is distinguished into four categories: laminar flow diffusion-based, geometric metering mixing-based, convection mixing-based, and static diffusion-based gradient generators.<sup>[147]</sup>

In addition to concentration gradients, other factors influence cell behavior and, as such, the accuracy of screening for new drugs. However, some of these factors are mechanical<sup>[148]</sup> and most CGGs cannot precisely adjust. Shourabi et al.<sup>[149]</sup> proposed an integrated microfluidic CGG capable of precisely controlling some mechanical factors, such as the ECM stiffness, shear stress, and osmotic pressure gradient. The proposed system is schematized in **Figure 10A**, consisting of two PDMS-layer microfluidic chips separated by a porous membrane. The upper membrane consists of two bubble trappers, a CGG, a membrane-based cell culturing chamber (MCCC), two inlets for the drugs, and a diluter (Figure 10B). The bottom membrane consists of a culture medium reservoir. The general operation scheme consists of the fluid introduction in the system, passing through the bubble trappers to eliminate the bubbles through

buoyancy force and encasing them in specific reservoirs. The drug is then diluted at four different concentrations, forming four distinct cell culturing chamber sections (including a control).<sup>[149]</sup>

The osmotic pressure gradients on cells are created because the fluid in the reservoir (bottom layer) acts as a basolateral fluid, while the flow of the MCCC (upper layer) acts as a luminal flow to be adjusted by varying the concentration of solutes in the reservoir. Furthermore, the porous substrate can be variable and adapted to the needs of cultured cell monolayers, allowing for adjusting ECM stiffness. The shear stress (adjusting the syringe pump's flow rate) can vary from 0 to 4 dyn cm<sup>-2</sup>, while the CGG maintains its function at various flow rates and concentrations, with a diffusion coefficient greater than  $5 \times 10^{10} \text{ m}^2 \text{ s}^{-1}$ .<sup>[149]</sup> Thus, this integrated microfluidic concentration gradient asserts itself as an easy-to-manufacture, low-cost, and high-throughput chip with the potential for studying different cell types in developing and screening new drugs.

Most described systems in the literature refer to dual gradient generators, not allowing the simultaneous study of the individual action and the interaction of two different drugs in a cell



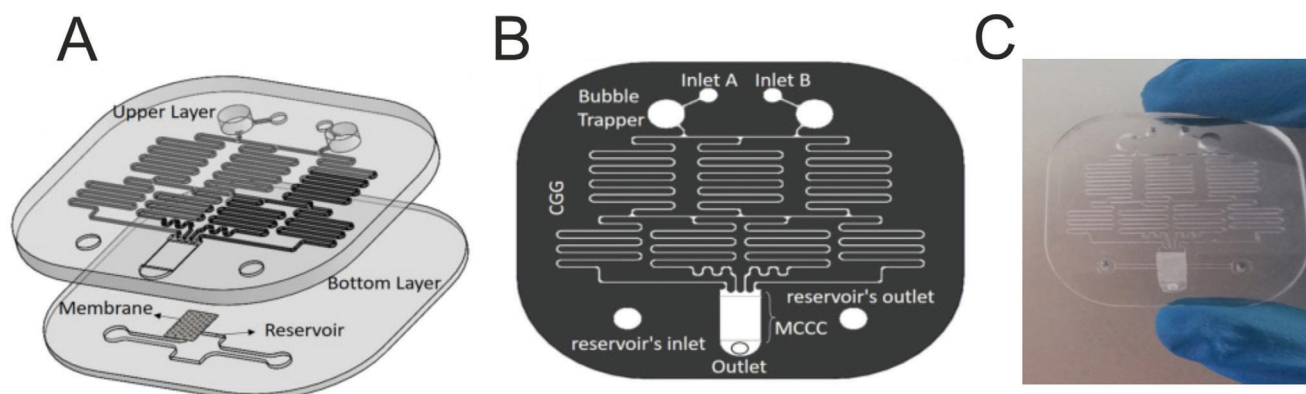


**Figure 10.** A) Schematic representation of the microfluidic platform design, consisting of two superimposed layers. B) Schematic representation of the upper layer constitution; and C) Photography of the actual microfluidic platform. Adapted with permission.<sup>[149]</sup> Copyright 2021, Elsevier.

line. Shen et al.<sup>[150]</sup> designed a device consisting of a new flow rate-independent microfluidic chip capable of including three controllable concentration gradients of multiple solutes. This device also allows to study of the individual effect of a drug or the joint action of two drugs on cell lines, aiming to create a personalized multicongcentration screening platform. This work follows advances<sup>[151]</sup> in which a high-efficiency fluid mixing system consisting of spiral microchannels was established to regulate Dean vortices that ensure the reduction of mixing lengths while increasing the mixing area. In a simplified way, the device is a three-set of gradient generators with compact double spiral mixers called  $\mu$ -TGSM.<sup>[150]</sup> The apparatus comprises twelve microchambers designed for cell-based assays when subjected to different concentrations of inserted drugs (inlets). The drug follows the structure of the microchannels designed to generate three concentration gradients. In **Figure 11A**, the gradual change of colors in the microchannels and microchambers is visible when a food dye is inserted in the respective inlet. Similar results were obtained with computer simulation (**Figure 11B**). The system was evaluated with two drugs, DXR and DDP, singly and combined for breast cancer MCF-7 and human hepatoma HepG2 cell lines.<sup>[150]</sup> Lower cell viability was observed in the higher concentration gradients, while the drug combination demonstrated a synergistic effect (**Figure 11C**). In agreement with the results obtained by conventional methods, this  $\mu$ -TGSM proved to be a promising device in the screening of drugs in a singular and combined way.<sup>[150]</sup>

In addition to being dependent on concentration, synergistic effect, and cell lines, some drugs also have activation or release schemes that add complexity to the discovery process. The screening platforms are also advantageous in including integrated analysis mechanisms in a single system. For instance, Lee et al.<sup>[152]</sup> developed a microfluidic system with light-intensity filters for drug screening for photodynamic therapy (**Figure 12A**). On this platform, the gradient generator constitutes an upper layer of the device, which works as an attenuating filter layer that controls the concentration of a color dye (**Figure 12B**). The color grading works as a light-intensity filter, allowing the study of eight light-intensity environments. At the same time, it is possible to vary the concentration of photosensitizer dosage.<sup>[152]</sup>

It demonstrated the platforms' ability as a screening tool for optimizing parameters of photodynamic therapy of cervical cancer cell line (HeLa) to determine the optimal experimental intensity. **Figure 12C** (top bright-field images) is representative of the culture chambers with HeLa cells and, without light irradiation, observed an adequate proliferation of the cells throughout the chamber. **Figure 12C** (bottom) shows the results of the photosensitizing activity of  $1.5 \mu\text{g mL}^{-1}$  PH (photosensitizer activated in photodynamic therapy with pulsed laser or light-emitting diode sources) under the action of light intensities from 0 to  $40 \text{ mW cm}^{-2}$ . The Live/Dead staining results (green/red, respectively) show increased dead cells with increasing light intensity. Using this experimental scheme, the authors evaluated eight light-intensity conditions in a single trial and repeated eight experiments for each condition.

Other applications include, for instance, rapid and high-throughput antimicrobial susceptibility testing. Azizi et al.<sup>[153]</sup> designed a novel gradient-based microchamber microfluidic platform that allows testing a broad spectrum of antibiotic concentrations in a single test. The authors tested it for profiling bacteria associated with bovine mastitis and human Crohn's disease, which completed the susceptibility test in only 3–4 h. Samandari et al.<sup>[154]</sup> developed a reusable and stand-alone PDMS-microfluidic generator directly attached to the cell culture plates, eliminating the need for surface pretreatment or additional coating. A case study with two breast cancer cell lines was performed, verifying that the platform guaranteed cellular behavior and functionality. Further, a differential invasion of cancer cells in response to generated chemical signals was confirmed. Finally, Lin et al.<sup>[155]</sup> combined a Darcy–Weisbach equation with computational fluid dynamics modeling to establish a method for developing a fluid shear stress (FSS) concentration gradient for the cellular microenvironment. This work was the first to combine these two parameters at a single-cell level and intends to enrich the fundamental knowledge of tumor development and respective therapeutic applications.

In conclusion, concentration gradient-based microfluidics demonstrates considerable potential as an integrated analysis of correlations between multiple parameters and drugs that dictate the biomedical action of drugs, which is required for a more efficient and effective selection for preclinical studies.

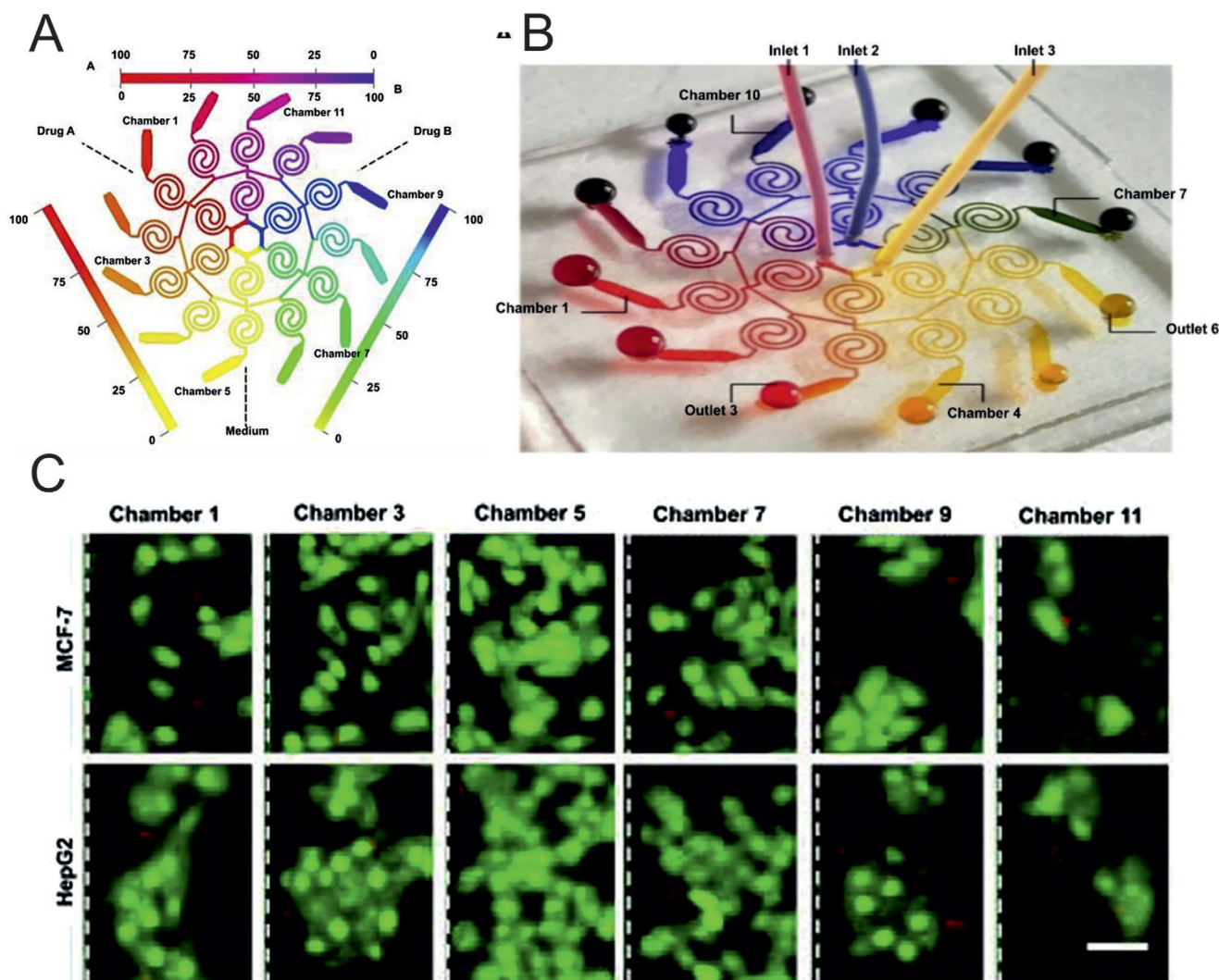


**Figure 11.** Microfluidics platform design for drug screening. A) Simulation of the concentration gradient formation with three food dye solutions (yellow, blue, and red) loaded from inlets located in the center of the device. B) Microfluidic device under the same conditions used in the test represented in (A), where it is possible to verify the consistency between the simulation and the actual result. C1, C4, C7, and C10 represent Chamber 1, Chamber 4, Chamber 7, and Chamber 10, respectively. C) staining fluorescence images of MCF-7 and HepG2 cells after continuous treatment with three drug-concentration gradients for 24 h. Scale bar, 100  $\mu\text{m}$ . Adapted with permission.<sup>[150]</sup> Copyright 2020, Elsevier.

#### 4.2. Droplet-Based Microfluidics

Droplet-based microfluidics is also a promising alternative to conventional drug screening, characterized by the ability to use water-in-oil (w/o) emulsion droplets to compartmentalize reactions within extremely small volumes, ranging from femto- to microliter.<sup>[156]</sup> Its versatility results from the ability of these systems to guarantee a high SAV ratio, rapid mixing, independent control of each drop, reduced reagents consumption, ability to split or merge drops to start or end reactions, and to produce a large number of monodisperse droplets.<sup>[103,156,157]</sup> The development of this technology is motivated by the interest in complementing the ability to produce droplets with well-defined and calibrated characteristics,<sup>[158]</sup> as well as its use as a lab-on-a-chip where the drops are studied as micro-reactors that confine the sample and allow the manipulation of small volumes.<sup>[158c,159]</sup>

Thus, controlling the droplet generation and their size and size distributions is essential for the proper functioning the devices and their adaptation to different applications. Droplet generation is ensured by passive and active methods (see ref. [160] for detailed information).

The three methodologies that dominate the formation of droplets are flow focusing, T-junctions, and co-flowing streams.<sup>[158c,161]</sup> They mainly differ in the flow field topology near the drop production zone.<sup>[158c]</sup> In flow focusing (Figure 13A), the droplet formation happens by breaking into elongation strained flows in which two counter-streaming flows squeeze the dispersed phase. In T-junctions (Figure 13B), the droplet is formed by breaking into cross-flowing streams in which two phases flowing through two orthogonal channels form droplets when they cross at 90° in the T-shaped junction. In coflowing (Figure 13C), two streams flowing in parallel near



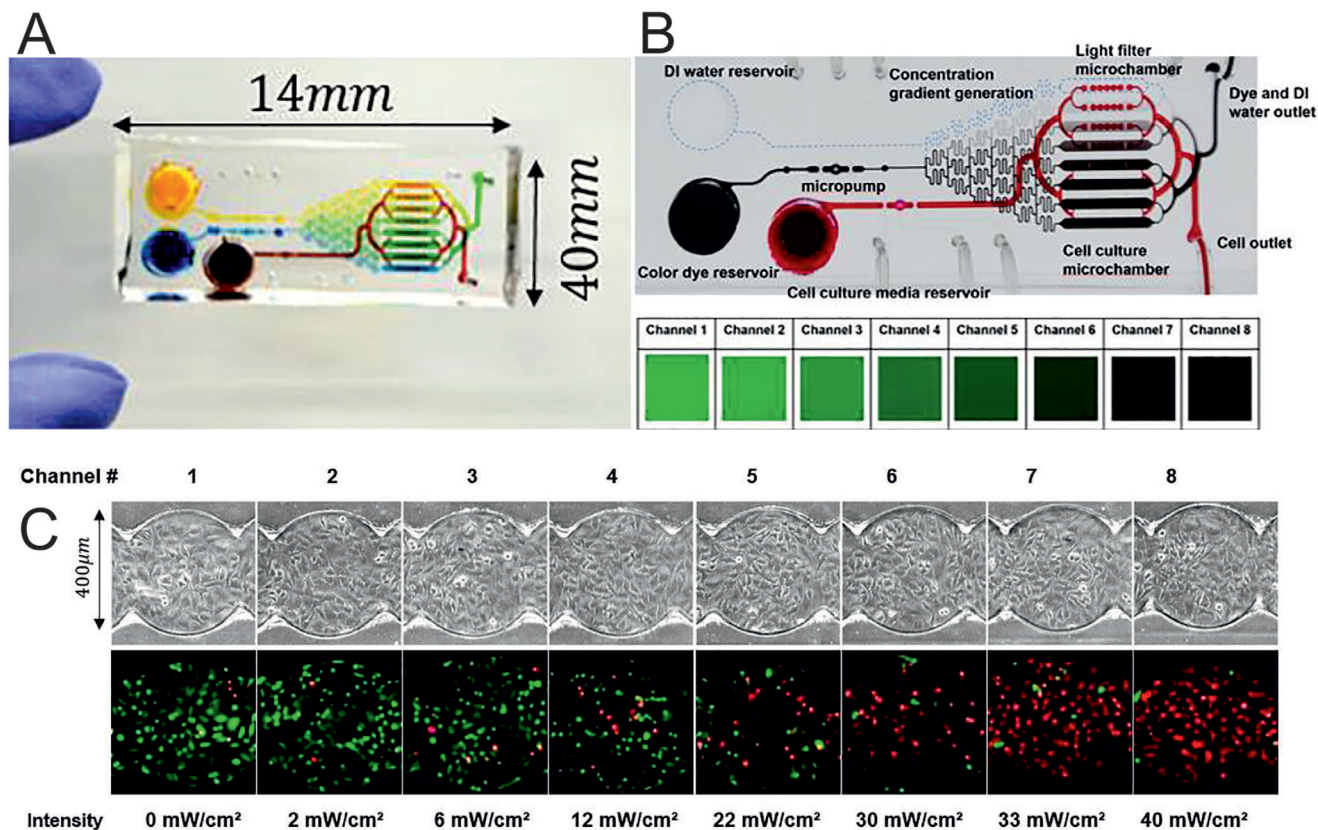


**Figure 12.** A) Photograph of the microfluidic system, injected with color dyes to reveal the inner structure. B) Microfluidic device demonstration employing red and black dyes (upper) and concentration gradient profile of a diffusive mixer using fluorescein isothiocyanate (bottom). C) Bright-field mosaic images of HeLa in culture chambers without light irradiation (upper) and corresponding live/dead fluorescence images of HeLa cells treated with 1  $\mu$ g mL<sup>-1</sup> photofrin (PH) with increasing light intensities from 0 to 40 mW cm<sup>-2</sup> (bottom). Adapted with permission.<sup>[152]</sup> Copyright 2022, Elsevier.

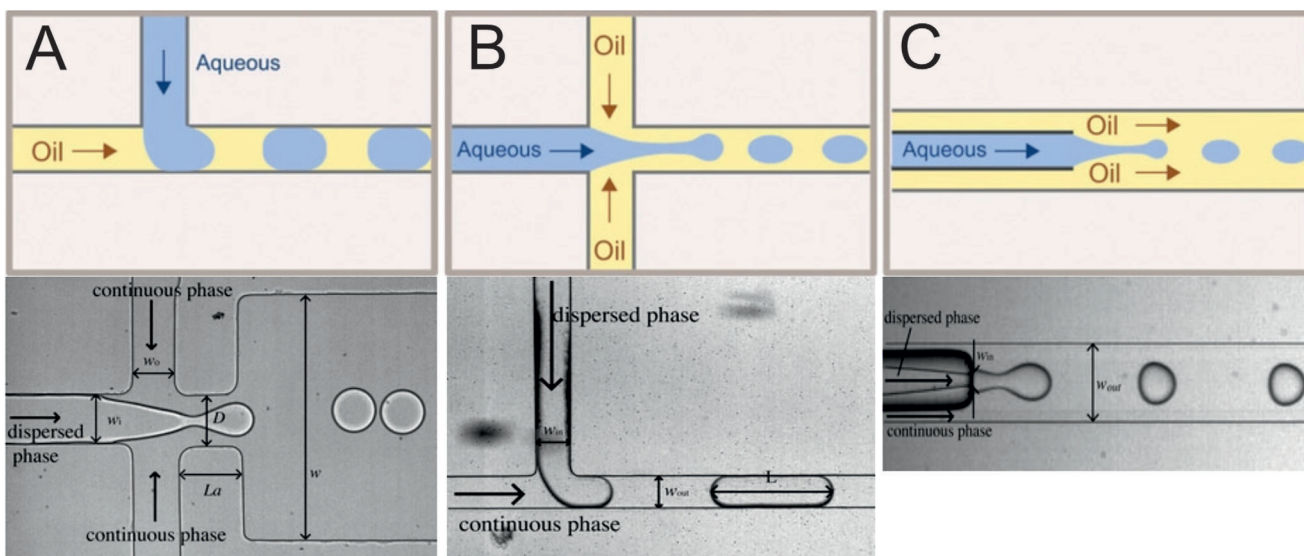


**Figure 13.** Schematic representation (top) and actual representation (bottom) of microfluidic droplet production using three distinct geometries: A) flow focusing; B) T-junction; and C) co-flowing. Adapted with permission.<sup>[158c,161]</sup> Copyright 2010 and 2020, the Royal Society of Chemistry and Wiley-VCH GmbH, respectively.

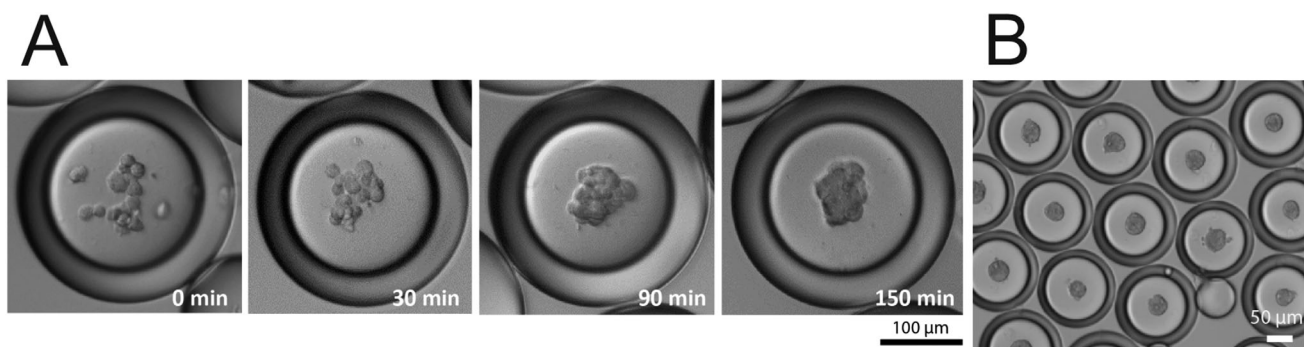


**Figure 14.** A) Time evolution of spheroid formation in DE droplets. Spheroids are formed in 150 min. B) Compact MSC spheroids in DE droplets after 6 h. Adapted with permission.<sup>[168]</sup> Copyright 2013, Springer Nature.

the nozzle squeeze the dispersed phase and lead to droplet formation.<sup>[158c,161]</sup>

Droplet-based microfluidics have allowed the scientific community to achieve revolutionary milestones in the biological analysis field, mainly in quantification at the single-cell level. For example, Klein et al.<sup>[162]</sup> developed a high-throughput droplet-microfluidic approach capable of single-cell capture, barcoding, and transcriptome profiling. In turn, Ben et al.<sup>[161]</sup> developed a device focused on single-cell tumor metabolomics to detect circulating tumor cells (CTCs). This cell type is a biomarker of metastasis progression and can also be associated with survival times. In this proof-of-concept, the authors could detect CTC in the blood of metastatic patients (with a precision of 10 tumor cells in a background of 200 000 white blood cells) through lactate concentration or acidification in the extracellular compartment of individual cells.<sup>[163]</sup>

As mentioned before, spheroids are 3D models that more closely reflect the cell-cell and cell-matrix relationship and in vivo interactions, facilitating drug screening.<sup>[164]</sup> However, the size and microenvironment of spheroids influence cell behavior and, as such, the response to drugs.<sup>[165]</sup> Although well-established, conventional methods,<sup>[166]</sup> although well established, make it challenging to produce spheroids with monodisperse sizes, have a low throughput, and make it difficult to supplement cues from the ECM.<sup>[167]</sup> Chan et al.<sup>[168]</sup> reported a two flow-focusing microfluidic device connected serially that generates water-in-oil-in-water (w/o/w) double-emulsion (DE) droplets where cells aggregate to form spheroids of controllable sizes (30–80 µm). The formation of MSC assembly spheroids was evaluated, which took place within 150 min (Figure 14A) due to confinement in droplets, promoting enhanced interactions between cells. Furthermore, the formed compact spheroids can be recovered by adding a droplet-releasing agent (Figure 14B). The formation of spheroids was also validated with the cell types of primary mouse embryonic fibroblasts (PMEF), a human hepatoma HepG2 (formation in 2 h), and Caco-2 (formation in 6 h).<sup>[168]</sup> These advances not only leverage the scale-up of spheroids production but also narrow the standardization of screening methods for new drugs.

Several research groups have attempted to reconstruct biologically relevant 3D structures within microfluidic droplets, which are especially important in mimicking the ECM for cancer drug screening. For example, Yu et al.<sup>[169]</sup> obtained MCSs using a core-shell structure incorporating ECM elements. The shell was algi-

nate, while the core was composed of collagen and Matrigel, in which the human breast cancer cells (MCF-7) dispersed to proliferate and form the spheroids. The spheroids' dose response was evaluated against two chemotherapeutic drugs, tamoxifen (TAM) and docetaxel (DTX). The spheroids showed drug resistance to TAM compared to conventional monolayer culture, while DTX results do not vary significantly. Sabhachandani et al.<sup>[170]</sup> developed a droplet-based microfluidics platform for high-throughput generation of hydrogel-based (alginate and puramatrix) 3D immunogenic diffuse large B cell lymphoma (DLBCL) spheroids. Figure 15A shows the schematic representation of the proposed droplet-based microfluidics platform. The device is coupled with a sphere-based microarray system capable of integrating and monitoring 250 cell-laden spheroids (Figure 15B). The platform has a T-junction geometry where droplets containing cells (cancer cells, fibroblasts, and lymphocytes) and liquid hydrogel (1% alginate and 0.15% puramatrix) are formed and driven to the docking array (Figure 15C,D). This platform enables the high-throughput generation of spheroids that mimic heterogeneity, complexity, and immune-rich tumor microenvironments. Furthermore, the spheroid array enables the continuous collection of cell-secreted factors, providing a multiparametric analysis of cellular interaction.

Droplet-based microfluidics platforms should also ensure the formation of droplets with appropriate compositions as the variation in the compositional chemistry of droplets interface can broaden their applicability spectrum. As a result, Bawazer et al.<sup>[171]</sup> proposed a novel high-throughput screening microfluidic strategy as a facilitating tool for engineering emulsions, aiming to easily identify oil/surfactant combinations to produce droplets for target applications.

The shape of the droplets must also be controlled or adapted to the type of application. However, the state-of-the-art mainly describes spherical droplets because of the tendency toward fluid equilibrium and minimization of interfacial free energy.<sup>[172]</sup> Although there is a higher production difficulty, nonspherical droplets have properties different from spherical ones (such as a larger surface area and anisotropic architectures). These new features can be beneficial, for instance, in the development of stimuli-responsive systems. Therefore, Gao et al.<sup>[173]</sup> presented a new method to produce protein-surfactant mono-dispersed droplets with nonspherical dimensions. The authors started by studying the effects of the S28C protein and its PEG-modified



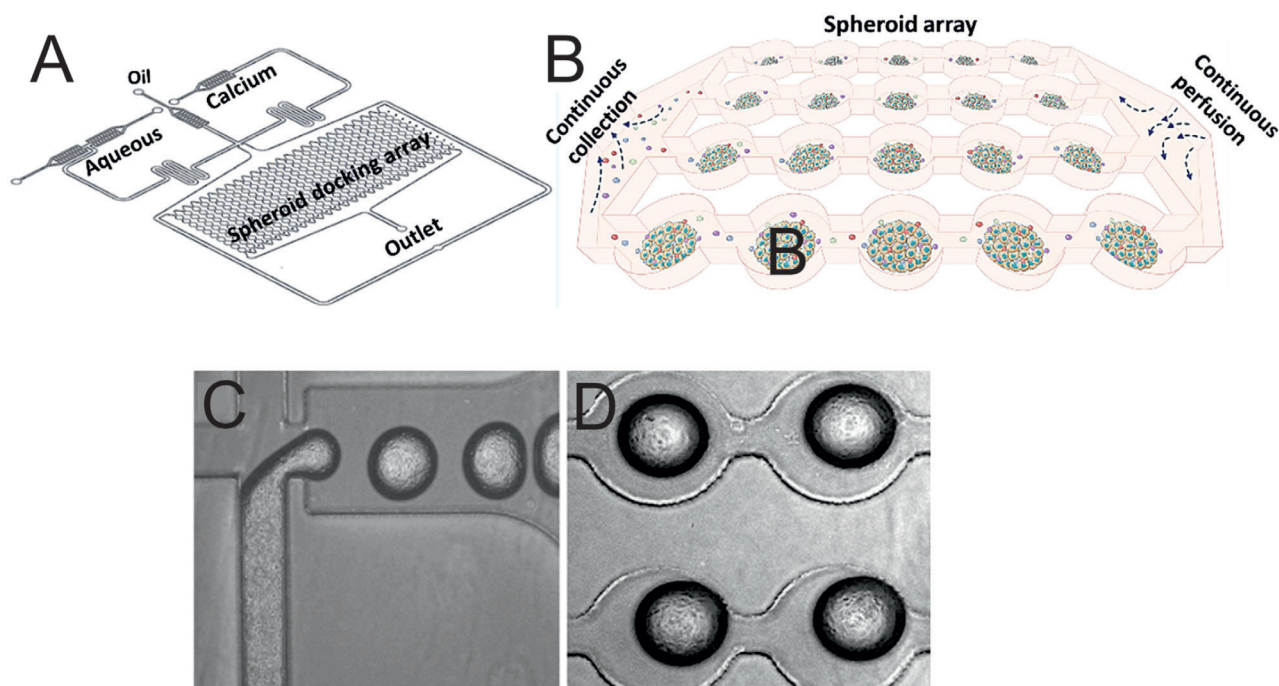


**Figure 15.** A) Schematic representation of the droplet-based microfluidics platform, coupled with B) sphere-based microarray system. C) Droplets containing cells and hydrogel are formed at the T-junction and D) driven to the docking array. Adapted with permission.<sup>[170]</sup> Copyright 2019, Elsevier.

form (S28C-PEG) as cosurfactants of a surface-active peptide (AM1 (Ac-MKQLADS LHQLARQ VSRLEHA-CONH<sub>2</sub>)) to produce stable droplets.

Nonetheless, it was discovered that PEG addition to S28C protein leads to changes in the mechanical properties of the protein film network. The oil droplets became “shape-memorable” with stronger interfacial networks, as they can maintain an ellipsoidal shape following deformation by the microfluidic channel.<sup>[173]</sup> The authors could produce nonspherical droplets with an aspect ratio between 1 and 3.4 by modifying the channel flow rate, while droplet size can be adjusted with additional channel designs.<sup>[173]</sup> This microfluidic approach can be used to create anisotropic compartments for biomimetic applications.

Other recent advances using droplet-based devices also include their use with high-throughput single-cell assays to study the antibiotic susceptibility of bacteria;<sup>[174]</sup> the conjugation of droplet microfluidics with lab-in-a-fiber device for virus detection;<sup>[175]</sup> in the sequencing of human immunodeficiency proviruses and the adjacent host junctions in individual cells to improve the genetic analysis of persistent HIV-infected cells;<sup>[176]</sup> the prototype of point-of-care (POC) device for easy blood coagulation monitoring assays in the clinic;<sup>[177]</sup> and automated clustered regularly interspaced short palindromic repeats (CRISPR)-based gene editing with high-throughput screening that allows the performance of 100 parallel reactions and six different mutations in a single chip.<sup>[178]</sup>

### 4.3. 3D-Printed Microfluidics

The combination of the advances in microfluidic platforms with the advantages of 3D-printed conformations complexity allows to take a step forward to the new era of drug screening.

Microfluidic devices are classified as symmetric fluidic gradients when they allow combining all the fluid input possibilities (Figure 16A). Conventional concentration gradient generators with two inputs are symmetrical, whereas those having three fluid inputs are nonsymmetrical as they do not produce all possible fluid combinations. Sweet and co-workers<sup>[179]</sup> developed a tetrahedrally arranged network of nodal combination–mixing–splitting units, allowing to achieve of a symmetric gradient of three or more fluid inputs (Figure 16B). This 3D microfluidic gradient generator was fabricated by employing multijet-3D-printed microchannel networks capable of three-fluid gradient generation for combination antimicrobial susceptibility testing (tetracycline, amikacin, and ciprofloxacin), as shown in Figure 16C.<sup>[179]</sup> The device aims to address the constraints of time-consuming and labor-intensive conventional techniques (≈2–4 d).<sup>[180]</sup> Furthermore, it intends to add functionalities to conventional concentration gradient generators, which are generally limited to 2D fluidic routing.

From a similar functional perspective, Chen et al.<sup>[181]</sup> proposed a 3D-printed microfluidic platform capable of generating 36 discrete concentration combinations to determine the optimal concentration of four drugs combined for cancer therapy. The multi-drug combination is crucial in cancer therapy as monotherapy has shown limited efficiency in several tumors due, among other factors, to the resistance created to conventional drugs. In addition, multi-drug combinations have demonstrated unique effects, including preventing growth and metastases while improving their efficiency with lower doses and, consequently, fewer side effects.<sup>[182]</sup> Figure 17A shows the proposed prototype of the microfluidic system and the respective computer-aided design (CAD) model. The system has four inlets and 36 outlets divided into four levels. Internally, it has an interconnected



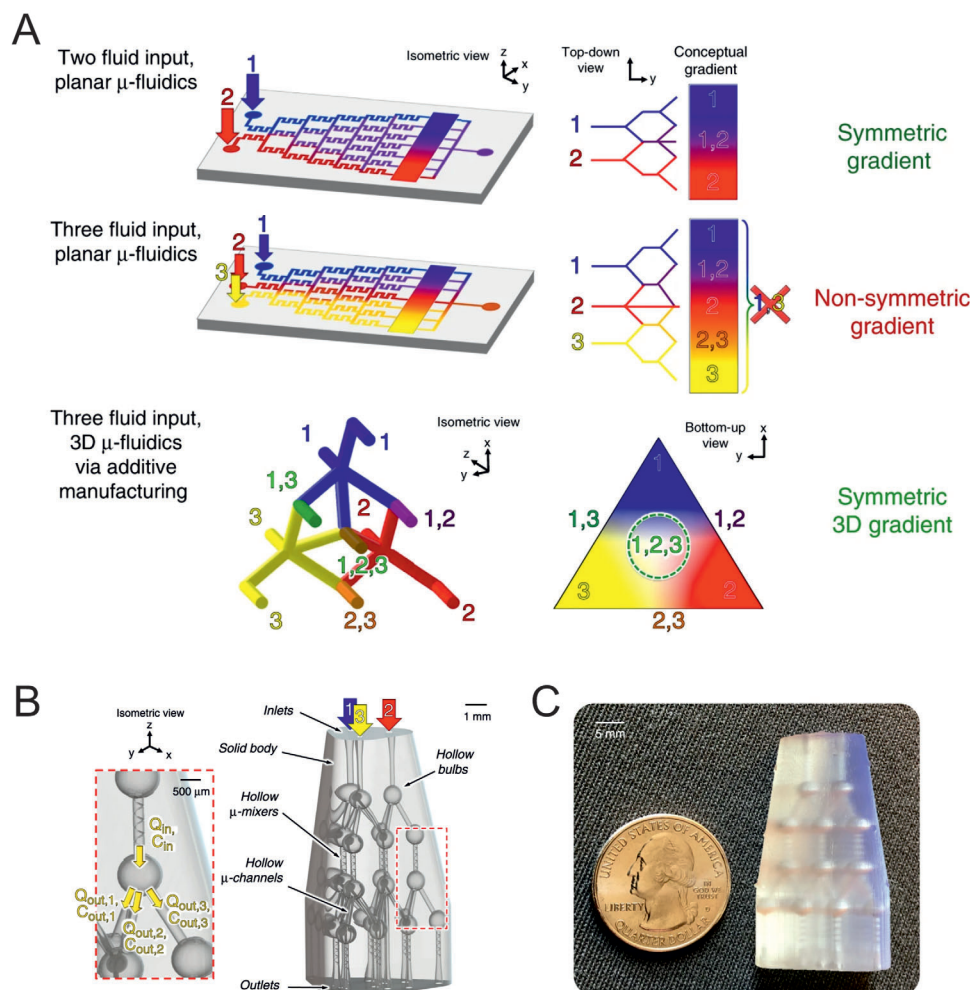


**Figure 16.** Schematic representation of conceptual microfluidic concentration gradient generators. A) Two fluid input planar devices allow combining all the fluid input possibilities, generating symmetric fluidic gradients; Three fluid input planar devices are limited to 2D fluidic processing, not allowing to make all combinations of fluid input and, therefore, generating nonsymmetric gradients; and three fluid input with truly 3D microchannel network, allowing to create symmetric 3D gradients of three or more input fluids. B) Schematic representation of the 3D microfluidic design composed of a single solid body with embedded hollow microchannel structures; inset: flow rates ( $Q_{in}$ ,  $Q_{out}$ ) and input species concentrations ( $C_{in}$ ,  $C_{out}$ ) into and out of each nodal unit; these variables are used in all analytical device output calculations; fluid inputs indicated by colored arrows. C) 3D  $\mu$ -CGG prototype after post-processing where the internal structures can be partially seen through the semi-transparent material (US quarter for scale). Adapted under the terms of the CC-BY-4.0 license.<sup>[179]</sup> Copyright 2020, the Authors. Published by Springer Nature.

microchannel network with a multi-layer tree-shaped branch unit with the dimensions shown in Figure 17B. The system is connected to a syringe pump and a collector with transparent silicone tube interconnects, which are then pipetted into 96-well plates for cytotoxicity analysis (Figure 17C).

The proof-of-concept was carried out using the drugs celecoxib (Celbx), 5-fluorouracil (5-FU), cyclophosphamide (CTX), and DXR and their effect on human lung cancer cell A549 activity evaluated.<sup>[181]</sup> Although the authors assume the need to optimize the device (namely to allow a large-scale concentration study), the preliminary results point to a significant advance in the state-of-the-art for multi-drug therapy devices.<sup>[181]</sup> Liu et al.<sup>[183]</sup> developed a novel 3D-printed nitrocellulose-based microfluidic chip as a stable oxygen gradient platform for cells that can generate a steady oxygen gradient for cells in 30 min. As oxygen is fundamental to biological processes, it is important to have an insight into the

effect of oxygen supply on cell behavior, particularly on the impact of hypoxia on cell growth and disease progression. This platform presents itself as a low-cost alternative for cell study, both as fundamental science and drug action study in mimetic environments.

The fabrication of devices that allow faster and more efficient drug screening must be followed by advances in new cell model development and methods to produce them.<sup>[184]</sup> In contrast to spheroids generated from single cell types or cell aggregates and represent tissues or parts of tissues, organoids refer to in vitro culture of tissue stem cells.<sup>[185]</sup> These structures can better mimic the in vivo environment when compared to spheroids since they recapitulate the organ of origin.<sup>[186]</sup> However, the growth of an organoid is a rigorous process that requires careful monitoring.<sup>[187]</sup> Thus, Khan et al.<sup>[188]</sup> developed a 3D-printed microfluidic bioreactor (using stereolithography-based

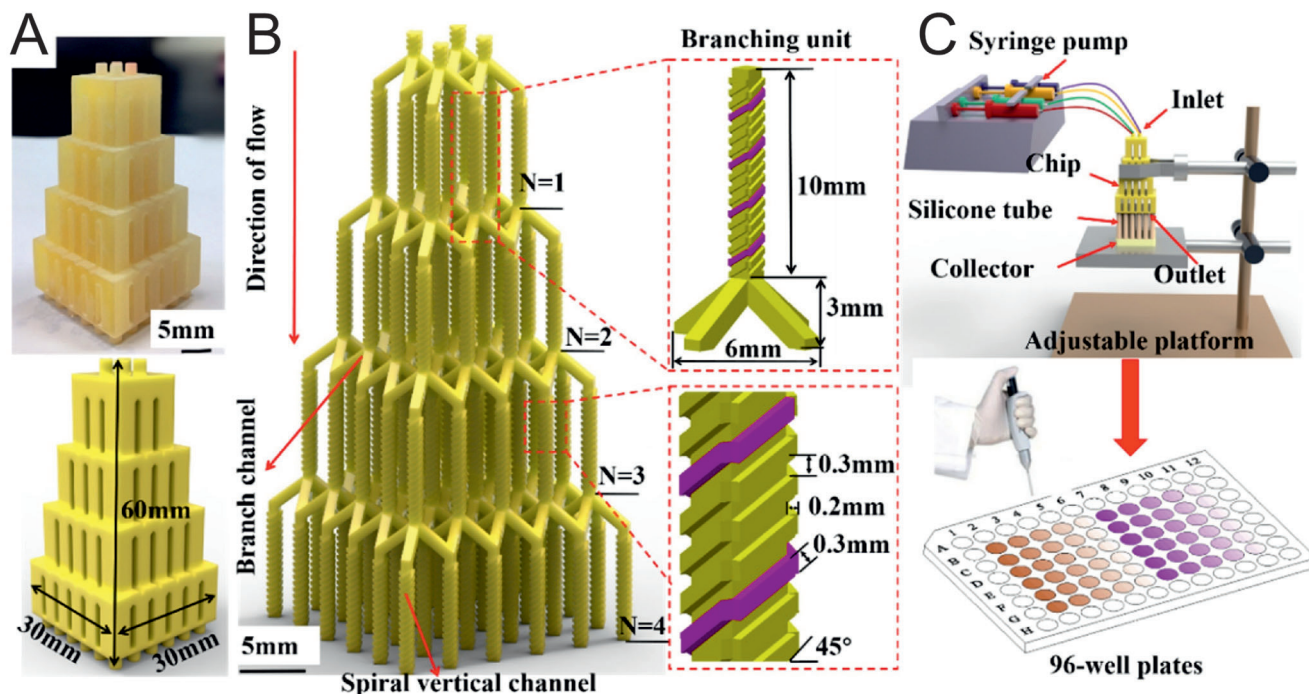


**Figure 17.** A) Prototype of the 3D-printed microfluidic chip and its respective CAD model. B) Internal architecture of the 3D-printed multi-drug combination gradient generator consists of an interconnected microchannel network with a multi-layer tree-shaped branch unit. Details and respective dimensions are shown on the right. C) Final assembly, in which the 3D-printed microfluidic chip is connected to a syringe pump and a collector with transparent silicone tube interconnects. Afterward, multidrug combinations are pipetted into 96-well plates for cytotoxicity analysis. Reproduced with permission.<sup>[181]</sup> Copyright 2018, Elsevier.

3D printing technology) that enables growth, in situ tracking, and live organoid imaging (Figure 18A). The viability of the growth of organoids in the microfluidic bioreactor compared to the regular culture was measured through the percentage of cells expressing the apoptotic marker cleaved caspase 3 (c-CASP3) and the proliferation marker Ki67. Figure 18B shows representative images of the two conditions. The ventricular zones (structures organized around a cavity or ventricle resembling the developing neocortex) can be observed in a yellow rectangle, and an orange rectangle marks the core region of organoids. Organoid growth took place over 7 d, and no significant difference in proliferative cells (pink) is visible. However, the organoids cultured in a microfluidic bioreactor showed a lower percentage of apoptotic cells (both in the ventricular zones and the core region). These results prove that the proposed system supports the viable development of organoids and that the continuous perfusion of the culture chamber decreases cell death in the organoid core. In addition to improved control over organoid production, the authors estimate a reduced price of around USD 5 per chip. The system can be improved by including more wells and integrating other functions, such as electrophysiology, for the model's comprehensive study.

The scientific community has hypothesized that the vascular network of organoids plays a key role in fate specification and morphogenesis. However, they are not intrinsically vascularized, and currently, existing vascularization strategies do not represent the spatial orientation and temporal synchronization found in vivo. Salmon et al.<sup>[189]</sup> described an approach for making human pluripotent stem cells (hPSC) interact with vascular cells

and produce vascularized organoids. The team developed a 3D-printed microfluidic chip that ensures sequential and developmentally matched coculture, allowing for spatial interaction between organoids and vasculature (Figure 19A). The microfluidic system has an "open well" design to allow the positioning of the organoid in the central compartment and its direct access for further characterization. This compartment is flanked by channels where vascular cells are seeded through an inlet. The communication between the organoid and the vascular cell in the channels is ensured by a nearly complete wall separating them, allowing their communication by the diffusion of molecules and cells (Figure 19B).

Other applications of this technology include protein quantification, sensing, biomarkers detection, and diagnosis. Sharafeldin et al.<sup>[190]</sup> developed a microfluidic microarray that lyses cells from oral cancer and quantifies membrane proteins, aiming for the detection of cancer metastasis. This platform quantifies the ultralow concentration of the metastatic biomarker of head and neck squamous cell carcinoma, desmoglein 3 (DSG3). On the other hand, Almughamsi et al.<sup>[191]</sup> developed a 3D-printed microfluidic platform with multiplexed immunoaffinity monolith extraction of preterm birth (defined as birth before 37 weeks of gestation) biomarkers. This device aims for the early diagnosis of preterm birth risk, which is challenging due to the low concentration of biomarkers in human blood serum. Wei et al.<sup>[192]</sup> developed a 3D-printed flexible epidermal microfluidic platform as a wearable bioanalytical device for sweat pH sensing.

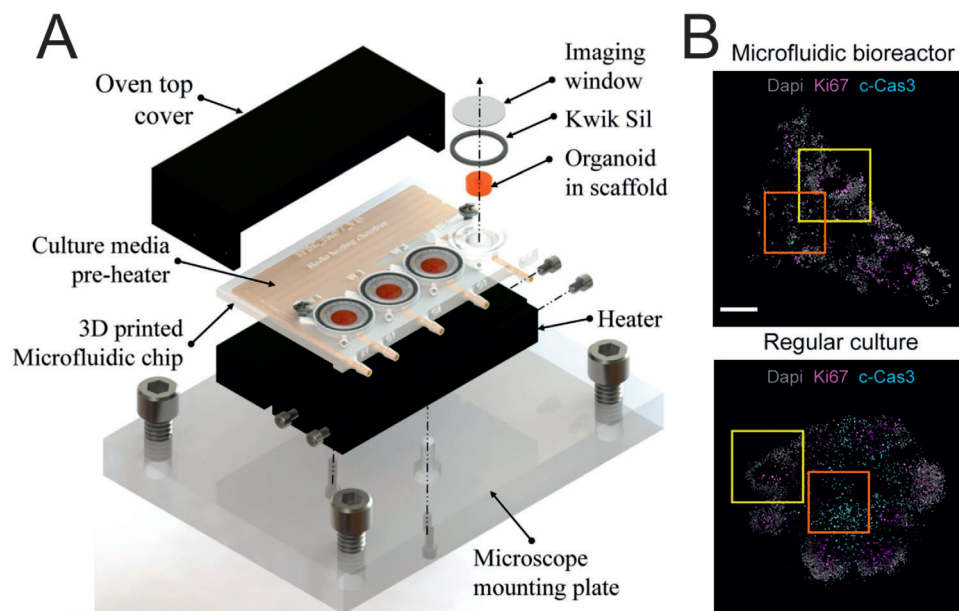


**Figure 18.** A) Microfluidic bioreactor assembly; B) Representative images of the viability of the growth of organoids in the microfluidic bioreactor compared (top) to the regular culture (bottom) labeled with the apoptotic marker c-Cas3 and the proliferation marker Ki67. Scale bar represents 200  $\mu\text{m}$ . Adapted with permission.<sup>[188]</sup> Copyright 2021, AIP Publishing.

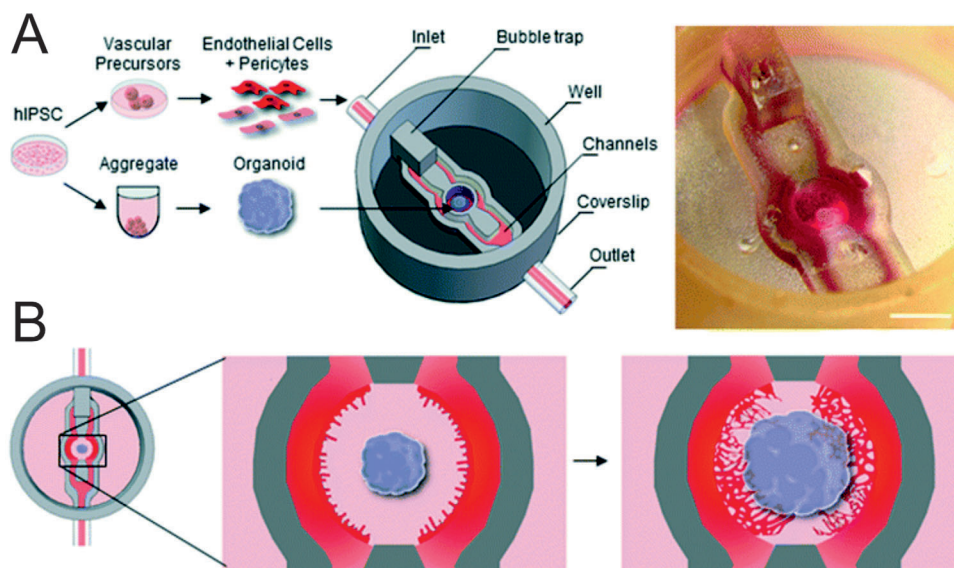


**Figure 19.** 3D-printed microfluidic platform. A) Left: schematic representation of hPSC differentiation into early organoids (then seeded in the central compartment) and into vascular cells (then seeded through the inlet to microfluidic channels). Right: stereomicroscopy image of the organoid on the microfluidic platform (scale: 2 mm). B) Schematic representation of angiogenic sprouting those results in organoid vascularization. Adapted with permission.<sup>[189]</sup> Copyright 2022, the Royal Society of Chemistry.

#### 4.4. Related Devices

The lack of standardized high-throughput systems for drug screening inspires the scientific community to develop several new devices that allow a more accurate, easier, and cheaper drug screening. Thus, in addition to the above approaches, other devices include digital-based microfluidics, SlipChip, and paper-based microfluidics.

In digital-based microfluidics,<sup>[193]</sup> discrete droplets are manipulated on an array of electrodes by applying electrical potentials between pairs of electrodes. The electronic control allows the automatic manipulation and analysis of individual droplets while avoiding the necessity of pumps or valves.<sup>[194]</sup> These devices have become a viable alternative to other liquid-handling techniques to generate and manipulate high-precision droplets.<sup>[195]</sup> Digital microfluidics cell-based applications are mainly categorized into



toxicity screening, cell sorting, and functional assays.<sup>[195]</sup> Zhai et al.<sup>[196]</sup> presented a digital microfluidic system with a control structure for droplet ejection from a drug dispenser (an electrode) by high-voltage pulse actuation. The device can deliver specific concentrations of a preloaded drug stock to the cell suspension (spanning three to four orders of magnitude) for single-drug and combinatorial multi-drug screening. The authors validated the system with two chemotherapeutic drugs, DDP and epirubicin (EPI), towards MDA-MB-231 breast cancer cells and MCF-10A normal breast cells. Recently, Zhang and Liu<sup>[197]</sup> developed digital microfluidics, including an electrochemical impedance spectroscopy (EIS)-based biosensor to detect human peripheral blood mononuclear cells to profile immune-mediated therapeutic responses.

Droplet-based microfluidics has evolved into an area called “controlled droplet microfluidics,” which concerns a set of techniques that perform multistep complex reaction protocols, using passive and automatic methods to control the flow that addresses droplets in series. The SlipChips are part of this category and are passive systems that perform multiplexed reactions without pumps or valves only by slipping two contacted substrates without requiring pump and valve controls.<sup>[198]</sup> This device consists of two plates that are in contact with each other. The bottom plate consists of an array of wells (where the reagents are placed) and disconnected ducts for loading. The top plate works as a cover for the bottom plate wells, containing an array of wells with a complementary pattern to the bottom plate. Chang and co-workers<sup>[199]</sup> developed a PDMS SlipChip, capable of culturing mammalian cells and performing multiple treatment assays. Since the transport of substances to the sample is based on a free-interface diffusion mechanism, it excludes the need for valves, pumps, and interconnections for flow control. Liu et al.<sup>[200]</sup> developed an instrument-free gradient-droplet SlipChip (gd-SlipChip) microfluidic device that generates gradient droplets by a surface tension-driven self-partitioning process. The device was effectively used for phenotypically determining *Escherichia coli* antimicrobial resistance profile. The minimal inhibitory concentration of *E. coli* was determined within 3 h of incubation. Recently, Catertton and co-workers<sup>[201]</sup> described the 3D printing of a SlipChip with a movable port for local stimulation of organ cultures.

In paper-based microfluidics, also called microfluidic paper-based analytical devices ( $\mu$ PADs), the devices are made from paper or another hydrophilic porous membrane by patterning paper with hydrophobic barriers to define hydrophilic channels and zones.<sup>[202]</sup> This technology is advantageous over commonly used polymer-based microfluidics (e.g., PDMS) because it is easier to fabricate, requires no pumps or external accessories, and is inexpensive and portable.<sup>[203]</sup> Furthermore, paper is advantageous concerning cell-based assays due to its reticulated structure, which offers a naturally 3D environment closer to the native cellular environment. As a result, paper-based microfluidics have been explored as a cell culture platform.<sup>[204]</sup> However, one of the drawbacks is that they can only achieve continuous perfusion by immersing the entire device in the cell culture medium. Therefore, most platforms reported for drug screening are limited to static analysis, not allowing a realistic investigation.<sup>[205]</sup> Therefore, Wu et al.<sup>[206]</sup> proposed a platform to control the continuous perfusion of paper-based microfluidics. The platform is printed with a low-cost 3D printer and ensures the continuous supply of

reagents to the  $\mu$ PADs, which absorbs the reagents by a capillary effect. The culture medium circulates under an external mechanical force provided by a peristaltic pump.

Fu et al.<sup>[207]</sup> developed a wick-like paper-based microfluidic device composed of folded paper strips that ensure medium self-driven perfusion. The platform consists of an upper layer used for cell culture in a standardized hydrophilic culture area, while the lower layer guarantees a medium supply according to the capillary phenomenon (Figure 20A). The device was validated by evaluating the cytotoxic effect of PTX, DXR, quercetin, and rutin on MCF-7 breast cancer cells and human hepatoma HepG2 cell lines by a smartphone-based colorimetric analysis system. Color intensity is related to cell viability, with lower viability corresponding to lighter colors. Figure 20B shows the variation in color intensity of different concentrations of PTX and DXR toward MCF-7 cells. Figure 20C shows the dose-response curves of MCF-7 breast cancer cells to these drugs, evidencing a cytotoxic effect dependent on the drug's concentration and showing the potential of these systems in drug screening.

## 5. Final Remarks and Outlook

Microfluidics-based cell culture platforms have a structural objective to give outright precision to the drug screening process while making it money, ethical, and time sustainable.

This review highlights the fundamental role that cell culture methods play in life research and development, as well as recent discoveries and technological advances in the area. More specifically, it focused on advances in cell-based drug screening on various microfluidics platforms, including concentration gradient-based microfluidics, droplet-based microfluidics, printed-based microfluidics, and digital-based microfluidics, SlipChip, and paper-based microfluidics. Relevant information from the reviewed works was compiled in Table 2, which compares the physicochemical and operational considerations of 2D cell culture, 3D cell culture, and microfluidics-based cell culture-related platforms.

An analysis of the table reveals that microfluidics-based cell culture platforms generally outperform conventional 2D and 3D cell culture methods. However, it should be highlighted that the lack of established protocols and validated models makes this alternative approach challenging to access. In addition, the preparation of devices is still primarily dependent on soft lithography, which requires specific infrastructure and, consequently, makes it labor, money, and time-consuming. Some of the production-associated challenges can be addressed by using 3D printing technology to manufacture microfluidic devices in a fast, one-step, low-cost, automatic, versatile way that allows for a possible high throughput fabrication of devices.<sup>[208]</sup> Furthermore, by sharing design files, replicating devices can be easily achieved between research groups. However, 3D printing still cannot replace soft-lithography and the advantages of PDMS. This is due to the unknown biocompatibility of most resins and plastics; solvent compatibility issues that lead to swelling of materials, causing flow problems;<sup>[209]</sup> semitransparent or translucent 3D printing materials, which complicated the observation process;<sup>[209,210]</sup> and finally, most of these materials are not gas permeable, making long-term cell culture within channels complicated.<sup>[93,210]</sup> In addition, soft-lithography is a well-established fabrication

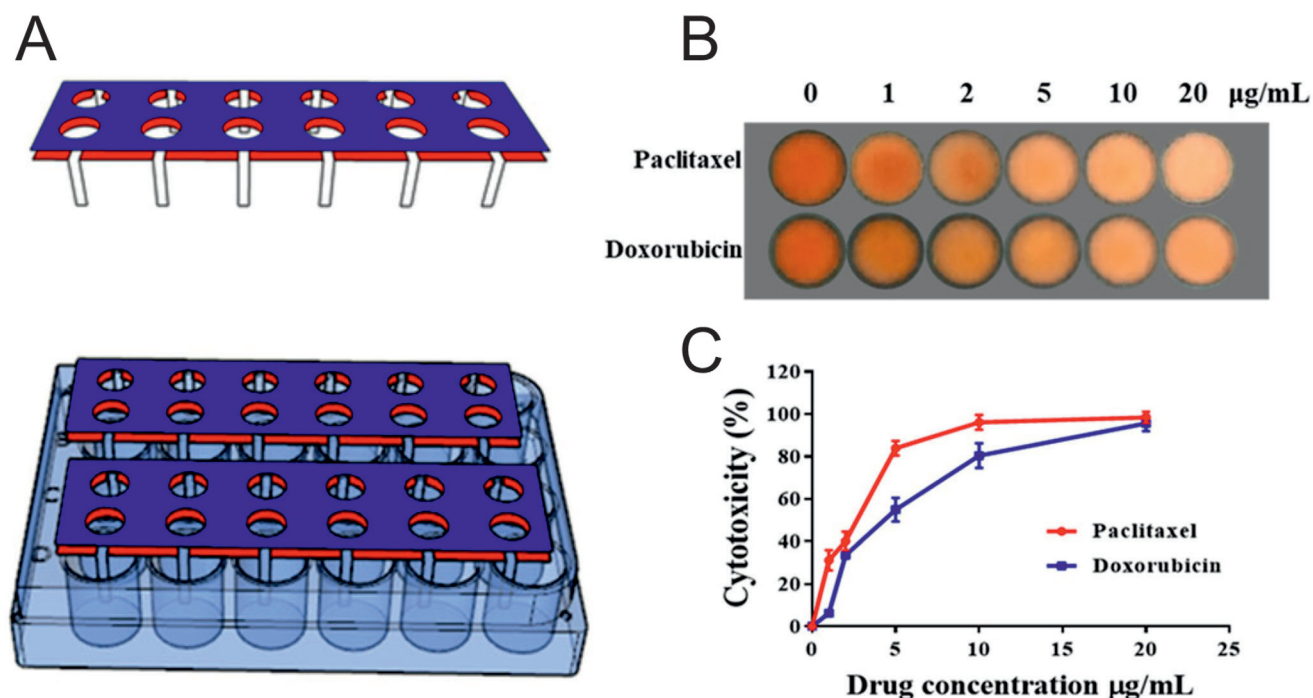


**Figure 20.** A) Schematic representation of the wick-like paper-based microfluidic device for high-throughput drug screening. B) Variation in color intensity of different concentrations of PTX and DXR towards MCF-7 cells; and C) respective dose-response curves. Adapted with permission.<sup>[207]</sup> Copyright 2021, Wiley-VCH GmbH.

**Table 2.** Comparative performance of the physicochemical and operational considerations of 2D cell culture, 3D cell culture, and microfluidics-based cell culture platforms.

	2D cell culture	3D cell culture	Gradient microfluidics	Droplet microfluidics	3D-printed microfluidics	Digital microfluidics	SlipChip	Paper microfluidics
Established protocols and validated models	+++	++	+	+	+	+	+	+
Operation difficulty	+	++	+++	+++	+++	++	++	+
Flexibility	x	x	X	x	x	x	x	+++
Reagents consumption	+++	+++	+	+	+	+	+	+
Heat transfer time	+++	+++	+	+	+	+	+	+
Volume density	+	+	+++	+++	+++	+++	+++	+++
Parallelization	x	+	+++	++	+++	+++	++	+
Dynamic control over culture nutrients and gases	+	+	+++	++	++	++	++	+
Control of mechanical factors	+	++	+++	+++	+++	+++	++	++
Simulations of in vivo microenvironment	+	++	+++	+++	+++	+++	+++	+
Multidrug combination	+	+	+++	++	+++	++	++	++
Multiparametric analysis	+	++	+++	+++	+++	+++	++	++
Observing cellular processes in real-time	+	+	++	+++	+	+++	++	+
Single-cell drug screening	x	x	++	+++	++	+++	+++	x
High-throughput screening	x	x	+++	++	+++	++	++	+
Money-consuming	++	+++	++	++	++	++	++	+

technique that enhances the device's manufacturing flexibility and functionality.

As a result, the platforms with the most significant potential for application in the pharmaceutical industry are PDMS concentration gradient-based microfluidics and droplet-based mi-

crofluidics. Concentration gradient-based microfluidics allows a high performance compared to traditional macroscale screening assays as they allow for precise control of stable concentration gradients (adjusting flow rate, channel structure, initial concentration) and expose cells to linear and nonlinear gradients.



Furthermore, the miniaturization of assays reduces reagent consumption. In addition, it provides controlled hydrodynamic and mass transport conditions, a greater spatiotemporal resolution, and a high SAV ratio that results in a lower heat transfer time and higher volume density. These platforms are beneficial in screening multiple drug candidates, simultaneously evaluating different concentrations, drug combinations, and the action of different regimens. However, one of the limitations of these devices is related to the high flow rate, whose fluid shear force can cause damage or cell death.

Regarding droplet-based microfluidics, the same advantages of the miniaturization effect can be pointed out as to the concentration gradient-based microfluidics. This method allows the production of highly monodisperse droplets, up to twenty thousand per second,<sup>[211]</sup> and the independent control of each droplet that works as a minireactor. These devices also allow the enclosure of a single cell in each droplet and form multiple identical minireactors in a short time, dominating the performance of single-cell drug screening and the parallelization of experimentation and processing. However, despite the advantages of compartmentalization, this characteristic raises some challenges related to maintaining a long-term cell culture, as it limits the supply of nutrients to the cells and other exchanges. Droplet generators can be purchased commercially; however, they require additional equipment, such as optical set-ups and pressure generators.<sup>[174]</sup>

Digital-based microfluidics is an alternative to droplet-based microfluidics that manipulate droplets through electrical or acoustic actuation without requiring pumps. This technology can individually and simultaneously manage several droplet compartments and be integrated with other technologies using simple instrumentation. Compared to conventional microfluidic droplet devices, these devices operate a smaller number of droplets (several up to tens), and the droplet volume is relatively larger (from microliters down to a hundred nanoliters).<sup>[212]</sup> However, the ability to configure and automate complex multistep operations makes these platforms a potential universal tool for drug screening.

SlipChip devices are an extension of microfluidic-based droplet devices that, without requiring pump and valve controls, demonstrate excellent efficiency in handling nanoliter-to-microliter aqueous samples.<sup>[213]</sup> In addition, this technique allows a series of analyses to be performed simultaneously, making this technique an asset for various screening applications. However, some limitations of this technique include the slow mixing of fluids and the inability of gases to diffuse freely through the glass substrates. However, it is an emerging technique whose straightforward operation should prompt investigators to face those challenges.

The differentiating advantages of paper-based microfluidics compared to other microfluidic devices are its flexibility, simple fabrication without cleanroom facilities, ease of operation without the need for pumps, and, above all, highly low-cost and easily accessible materials.<sup>[202a]</sup> Furthermore, its structure facilitates 3D mimicry of the cells' native cellular environment. However, the use of these platforms is conditioned by their limitation to static analysis, inability to form droplets and manipulate cells in paper-based channels, difficulty recovering samples or collecting products, and the structural variability of paper fibers that introduces undetermined errors in drug screening. Furthermore, pa-

per is not optically transparent, and the autofluorescence of paper substrates makes fluorescent imaging difficult, which is the most used technique for cell response analysis. Therefore, paper-based microfluidics will significantly benefit from the standardization of manufacturing methods and their integration with other microfluidic (digital-based microfluidics) platforms that are effective as a basis for mixing and processing fluids.<sup>[214]</sup>

In conclusion, the potential that microfluidic cell culture adds to the well-established macroscopic cell culture is undoubted. It allows the scientific community to gain insights into molecular and cellular biology and perform high-throughput drug screening that would otherwise be extremely difficult with macroscopic cell culture techniques. However, there is still a long way to go to understand all the differences in cellular behavior between microfluidic and macroscopic cell cultures since science is, until now, mainly supported by the knowledge generated in macroscopic methods. Moreover, although microfluidic devices already allow a good mimicry of the physiological microenvironment, this area must continually grow to increase the simulation of the human body in a holistic and consolidated way. These developments must be monitored multidisciplinary, and engineering must play a key role in developing detectors or automatic analysis systems integrated into the devices for real-time analysis of cellular responses. It is intended that future generations of microfluidic devices for pharmaceutical research will allow the replacement of ethically and economically in vivo assays and bring society closer to personalized medicine, which will occur only by crossing the challenging academia to industry barrier for their standardization, adoption, and commercialization.

## Acknowledgements

This work was supported by FCT - Fundação para a Ciência e Tecnologia (FCT) under the scope of the strategic funding UIDB/04650/2020, UIDP/04650/2020, UIDB/04436/2020, UIDP/04436/2020. The authors also thank FCT for financial support under grant SFRH/BD/141936/2018 (B.D.C.) and the contract under the Stimulus of Scientific Employment 2020.02304.CEECIND (V.C.). The authors also acknowledge funding by Spanish State Research Agency (AEI) and the European Regional Development Fund (ERFD) through the project PID2019-106099RB-C43/AEI/10.13039/501100011033 and from the Basque Government Industry Departments under the ELKARTEK program.

## Conflict of Interest

The authors declare no conflict of interest.

## Keywords

biomimetics, cell cultures, cells-on-a-chip, drug screening, microfluidics

Received: November 14, 2022

Revised: February 27, 2023

Published online: March 20, 2023

[1] G. M. Whitesides, *Nature* **2006**, 442, 368.

[2] A. Manz, E. Verpoorte, D. E. Raymond, C. S. Effenhauser, N. Burggraf, H. M. Widmer, in *Micro Total Analysis Systems* (Eds: A. Van

- den Berg, P. Bergveld), Springer, Dordrecht, the Netherlands, **1995**, pp. 5–27.
- [3] H. A. Stone, A. D. Stroock, A. Ajdari, *Annu. Rev. Fluid Mech.* **2004**, 36, 381.
- [4] P. Gravesen, J. Branebjerg, O. S. Jensen, *J. Micromech. Microeng.* **1993**, 3, 168.
- [5] T. M. Squires, S. R. Quake, *Rev. Mod. Phys.* **2005**, 77, 977.
- [6] J. Zhang, S. Yan, D. Yuan, G. Alici, N.-T. Nguyen, M. E. Warkiani, W. Li, *Lab Chip* **2016**, 16, 10.
- [7] Z. Li, B. Zhang, D. Dang, X. Yang, W. Yang, W. Liang, *Sens. Actuators, A* **2022**, 344, 113757.
- [8] C.-C. Lee, G. Sui, A. Elizarov, C. J. Shu, Y.-S. Shin, A. N. Dooley, J. Huang, A. Daridon, P. Wyatt, D. Stout, *Science* **2005**, 310, 1793.
- [9] D. Lombardi, P. S. Dittich, *Expert Opin. Drug Discovery* **2010**, 5, 1081.
- [10] A. Buguin, Y. Chen, P. Silberzan, in *Nanoscience: Nanobiotechnology and Nanobiology*, Springer, Berlin **2009**, pp. 743–774.
- [11] Y. Jin, M. Dou, S. Zhuo, Q. Li, F. Wang, J. Li, *Food Control* **2022**, 136, 108885.
- [12] a) D. Park, H. Kim, J. W. Kim, *Biomicrofluidics* **2021**, 15, 051302; b) M.-H. Lee, S.-G. Oh, S.-K. Moon, S.-Y. Bae, *J. Colloid Interface Sci.* **2001**, 240, 83.
- [13] a) M. R. Sarabi, D. Yigci, M. M. Alseed, B. A. Mathyk, B. Ata, C. Halicigil, S. Tasoglu, *iScience* **2022**, 25, 104986; b) P. Yager, T. Edwards, E. Fu, K. Helton, K. Nelson, M. R. Tam, B. H. Weigl, *Nature* **2006**, 442, 412.
- [14] M. M. Gong, D. Sinton, *Chem. Rev.* **2017**, 117, 8447.
- [15] D. Zhang, C. Li, D. Ji, Y. Wang, *Crit. Rev. Anal. Chem.* **2022**, 52, 1432.
- [16] a) A. Carrel, *J. Exp. Med.* **1912**, 16, 165; b) W. Jacoby, I. Pasten, in *Methods in enzymology*, Academic Press, New York **1979**.
- [17] K. Jaroch, A. Jaroch, B. Bojko, *J. Pharm. Biomed. Anal.* **2018**, 147, 297.
- [18] S. M. Bhatt, *Animal Cell Culture: Concept and Application*, Alpha Science International Ltd, Oxford, UK **2011**.
- [19] M. L. Andersen, L. M. Winter, *An. Acad. Bras. Cienc.* **2017**, 91, e20170238.
- [20] F. Pampaloni, E. G. Reynaud, E. H. Stelzer, *Nat. Rev. Mol. Cell Biol.* **2007**, 8, 839.
- [21] J. Sibbitts, K. A. Sellens, S. Jia, S. A. Klasner, C. T. Culbertson, *Anal. Chem.* **2018**, 90, 65.
- [22] S. Battat, D. A. Weitz, G. M. Whitesides, *Lab Chip* **2022**, 22, 530.
- [23] T. A. Duncombe, A. M. Tentori, A. E. Herr, *Nat. Rev. Mol. Cell Biol.* **2015**, 16, 554.
- [24] P. De Stefano, E. Bianchi, G. Dubini, *Biomicrofluidics* **2022**, 16, 031501.
- [25] a) N. V. Menon, S. B. Lim, C. T. Lim, *Curr. Opin. Pharmacol.* **2019**, 48, 155; b) Y. Shi, Y. Cai, Y. Cao, Z. Hong, Y. Chai, *TrAC, Trends Anal. Chem.* **2021**, 134, 116118; c) J. Radhakrishnan, S. Varadaraj, S. K. Dash, A. Sharma, R. S. Verma, *Drug Discovery Today* **2020**, 25, 879; d) F. Dabbagh Moghaddam, F. Romana Bertani, *Mater. Chem. Horiz.* **2022**, 1, 69.
- [26] S. K. Kim, Y. H. Kim, S. Park, S.-W. Cho, *Acta Biomater.* **2021**, 132, 37.
- [27] D. Liu, M. Sun, J. Zhang, R. Hu, W. Fu, T. Xuanyuan, W. Liu, *Analyst* **2022**, 147, 2294.
- [28] Z. Fangjuan, L. Haibing, G. Mengqi, W. Defu, N. Yanbing, S. Shaofei, *Prog. Chem.* **2021**, 33, 1138.
- [29] J. A. DiMasi, L. Feldman, A. Seckler, A. Wilson, *Clin. Pharmacol. Ther.* **2010**, 87, 272.
- [30] R. C. Mohs, N. H. Greig, *Alzheimer's Dementia: Transl. Res. Clin. Interventions* **2017**, 3, 651.
- [31] W. N. Hait, *Nat. Rev. Drug Discovery* **2010**, 9, 253.
- [32] J. Drews, *Science* **2000**, 287, 1960.
- [33] R. G. Harrison, M. Greenman, F. P. Mall, C. Jackson, *Anat. Rec.* **1907**, 1, 116.
- [34] a) E. Michelini, L. Cevenini, L. Mezzanotte, A. Coppa, A. Roda, *Anal. Bioanal. Chem.* **2010**, 398, 227; b) R. Zang, D. Li, I.-C. Tang, J. Wang, S.-T. Yang, *Int. J. Biotechnol. Wellness Ind.* **2012**, 1, 31.
- [35] J. A. DiMasi, H. G. Grabowski, R. W. Hansen, *J. Health Econ.* **2016**, 47, 20.
- [36] S. A. Sundberg, *Curr. Opin. Biotechnol.* **2000**, 11, 47.
- [37] a) S. Yang, R. Ng, *Mater. Today* **2007**, 10, 64; b) C. Jensen, Y. Teng, *Front. Mol. Biosci.* **2020**, 7, 33.
- [38] L. J. Bonassar, C. A. Vacanti, *J. Cell. Biochem.* **1998**, 72, 297.
- [39] R. Edmondson, J. J. Broglie, A. F. Adcock, L. Yang, *Assay Drug Dev. Technol.* **2014**, 12, 207.
- [40] V. M. Weaver, S. Lelièvre, J. N. Lakin, M. A. Chrenek, J. C. Jones, F. Giaccotti, Z. Werb, M. J. Bissell, *Cancer Cell* **2002**, 2, 205.
- [41] a) B. Weigelt, C. M. Ghajar, M. J. Bissell, *Adv. Drug Delivery Rev.* **2014**, 69, 42; b) S. A. Langhans, *Front. Pharmacol.* **2018**, 9, 6.
- [42] M. Prieto-Vila, R.-u. Takahashi, W. Usuba, I. Kohama, T. Ochiya, *Int. J. Mol. Sci.* **2017**, 18, 2574.
- [43] C. Bonnans, J. Chou, Z. Werb, *Nat. Rev. Mol. Cell Biol.* **2014**, 15, 786.
- [44] a) B. Han, C. Qu, K. Park, S. F. Konieczny, M. Korc, *Cancer Lett.* **2016**, 380, 319; b) S. Li, K. Yang, X. Chen, X. Zhu, H. Zhou, P. Li, Y. Chen, Y. Jiang, T. Li, X. Qin, *Biofabrication* **2021**, 13, 045013.
- [45] M. E. Fiori, S. Di Franco, L. Villanova, P. Bianca, G. Stassi, R. De Maria, *Mol. Cancer* **2019**, 18, 70.
- [46] a) S. Das, B. Shapiro, E. A. Vucic, S. Vogt, D. Bar-Sagi, *Cancer Res.* **2020**, 80, 1088; b) Y. Qiao, C. Zhang, A. Li, D. Wang, Z. Luo, Y. Ping, B. Zhou, S. Liu, H. Li, D. Yue, *Oncogene* **2018**, 37, 873.
- [47] a) G. B. Bradford, B. Williams, R. Rossi, I. Bertoncello, *Exp. Hematol.* **1997**, 25, 445; b) M. E. Fiori, L. Villanova, R. De Maria, *Curr. Opin. Pharmacol.* **2017**, 35, 1.
- [48] a) C. Migone, in *Three-dimensional polymeric systems for cancer cells studies*, University of Pisa, Toscana, Italy **2014**; b) J. Debnath, J. S. Brugge, *Nat. Rev. Cancer* **2005**, 5, 675.
- [49] a) F. M. Kievit, S. J. Florczyk, M. C. Leung, K. Wang, J. D. Wu, J. R. Silber, R. G. Ellenbogen, J. S. Lee, M. Zhang, *Biomaterials* **2014**, 35, 9137; b) C. Liu, Y. Liu, X.-X. Xu, H. Wu, H.-G. Xie, L. Chen, T. Lu, L. Yang, X. Guo, G.-W. Sun, *Exp. Cell Res.* **2015**, 330, 123.
- [50] W. Yang, Z. Wang, T. Yu, Y. Chen, Z. Ge, *Sens. Actuators, A: Physical* **2021**, 333, 113229.
- [51] a) S. Maramizonou, X. Tao, M. Rahmati, C. Jia, R. Tao, H. Torun, T. Zheng, H. Jin, S. Dong, J. Luo, *Int. J. Mech. Sci.* **2021**, 202, 106536; b) Q. Cao, Q. Fan, Q. Chen, C. Liu, X. Han, L. Li, *Mater. Horiz.* **2020**, 7, 638; c) Y.-S. Chen, C.-K. Tung, T.-H. Dai, X. Wang, C.-T. Yeh, S.-K. Fan, C.-H. Liu, *Sens. Actuators, B* **2021**, 343, 130159; d) Y. Song, Q. Tian, J. Liu, W. Guo, Y. Sun, S. Zhang, *Lab Chip* **2021**, 21, 1590.
- [52] a) W. Yang, H. Yu, Y. Wang, L. Liu, presented at 2016 IEEE 16th Int. Conf. on Nanotechnology (IEEE-NANO), Sendai, Japan, August **2016**; b) M. Garcia-Hernando, A. Calatayud-Sanchez, J. Etxebarria-Elezgarai, M. M. de Pancorbo, F. Benito-Lopez, L. Basabe-Desmonts, *Anal. Chem.* **2020**, 92, 9658; c) J. Park, J. H. Choi, S. Kim, I. Jang, S. Jeong, J. Y. Lee, *Acta Biomater.* **2019**, 97, 141; d) R. Piya, Y. Zhu, A. H. Soeriyadi, S. M. Silva, P. J. Reece, J. J. Gooding, *Biosens. Bioelectron.* **2019**, 127, 229.
- [53] a) Y. Hou, W. Xie, K. Achazi, J. L. Cuellar-Camacho, M. F. Melzig, W. Chen, R. Haag, *Acta Biomater.* **2018**, 77, 28; b) J. Zhang, Y. Luo, C. L. Poh, *J. Mol. Biol.* **2020**, 432, 3137.
- [54] a) M. Li, L. Liu, N. Xi, Y. Wang, *IEEE Trans. Nanotechnol.* **2017**, 16, 217; b) H. Zhong, L. Xuan, D. Wang, J. Zhou, Y. Li, Q. Jiang, *RSC Adv.* **2017**, 7, 21837.
- [55] H. L. Hadden, C. A. Henke, *Am J. Respir. Crit. Care Med.* **2000**, 162, 1553.
- [56] D. E. Discher, P. Janmey, Y.-L. Wang, *Science* **2005**, 310, 1139.
- [57] J. Lee, O. Jeon, M. Kong, A. A. Abdeen, J.-Y. Shin, H. N. Lee, Y. B. Lee, W. Sun, P. Bandaru, D. S. Alt, *Sci. Adv.* **2020**, 6, eaaz5913.
- [58] J. M. Stukel, R. K. Willits, *Biomed. Mater.* **2018**, 13, 024102.

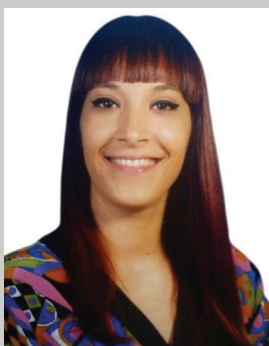
- [59] J. C. Dunn, M. L. Yarmush, H. G. Koebe, R. G. Tompkins, *FASEB J.* **1989**, *3*, 174.
- [60] M. Vinken, *Curr. Opin. Toxicol.* **2021**, *25*, 1.
- [61] R. Utoh, S. Enomoto, M. Yamada, K. Yamanaka, Y. Yajima, K. Furusawa, M. Seki, *Mater. Sci. Eng., C* **2021**, *129*, 112417.
- [62] a) A. Kaneko, Y. Sankai, *PLoS One* **2014**, *9*, e102703; b) G. J. Brewer, C. W. Cotman, *Brain Res.* **1989**, *494*, 65.
- [63] K. Duval, H. Grover, L.-H. Han, Y. Mou, A. F. Pegoraro, J. Fredberg, Z. Chen, *Physiology* **2017**, *32*, 266.
- [64] a) M. Kapałczyńska, T. Kolenda, W. Przybyła, M. Zajączkowska, A. Teresiak, V. Filas, M. Ibbs, R. Bliźniak, Ł. Łuczewski, K. Lamperska, *Arch. Med. Sci.* **2018**, *14*, 910; b) B. A. Justice, N. A. Badr, R. A. Felder, *Drug Discovery Today* **2009**, *14*, 102.
- [65] a) E. C. Costa, A. F. Moreira, D. de Melo-Diogo, V. M. Gaspar, M. P. Carvalho, I. J. Correia, *Biotechnol. Adv.* **2016**, *34*, 1427; b) S. Suri, C. E. Schmidt, *Tissue Eng., Part A* **2010**, *16*, 1703.
- [66] a) K. R. King, C. C. J. Wang, M. R. Kaazempur-Mofrad, J. P. Vacanti, J. T. Borenstein, *Adv. Mater.* **2004**, *16*, 2007; b) C. J. Bettinger, E. J. Weinberg, K. M. Kulig, J. P. Vacanti, Y. Wang, J. T. Borenstein, R. Langer, *Adv. Mater.* **2006**, *18*, 165; c) J. T. Borenstein, M. M. Tupper, P. J. Mack, E. J. Weinberg, A. S. Khalil, J. Hsiao, G. García-Cardena, *Biomed. Microdevices* **2010**, *12*, 71; d) J. Wang, C. J. Bettinger, R. S. Langer, J. T. Borenstein, *Organogenesis* **2010**, *6*, 212.
- [67] X. Li, A. V. Valadez, P. Zuo, Z. Nie, *Bioanalysis* **2012**, *4*, 1509.
- [68] L. Kim, Y.-C. Toh, J. Voldman, H. Yu, *Lab Chip* **2007**, *7*, 681.
- [69] S. J. Florczyk, G. Liu, F. M. Kievit, A. M. Lewis, J. D. Wu, M. Zhang, *Adv. Healthcare Mater.* **2012**, *1*, 590.
- [70] C. Frantz, K. M. Stewart, V. M. Weaver, *J. Cell Sci.* **2010**, *123*, 4195.
- [71] a) M. Sepantafar, R. Maheronnaghsh, H. Mohammadi, F. Radmanesh, M. M. Hasani-Sadrabadi, M. Ebrahimi, H. Baharvand, *Trends Biotechnol.* **2017**, *35*, 1074; b) T. Debnath, S. Ghosh, U. S. Potlapuvu, L. Kona, S. R. Kamaraju, S. Sarkar, S. Gaddam, L. K. Chelluri, *PLoS One* **2015**, *10*, e0120803.
- [72] D. S. Benoit, M. P. Schwartz, A. R. Durney, K. S. Anseth, *Nat. Mater.* **2008**, *7*, 816.
- [73] a) S. R. Caliari, J. A. Burdick, *Nat. Methods* **2016**, *13*, 405; b) N. C. Hunt, D. Hallam, A. Karimi, C. B. Mellough, J. Chen, D. H. Steel, M. Lako, *Acta Biomater.* **2017**, *49*, 329; c) G. Hochleitner, F. Chen, C. Blum, P. D. Dalton, B. Amsden, J. Groll, *Acta Biomater.* **2018**, *72*, 110.
- [74] a) C. Zhao, Y. Li, G. Peng, X. Lei, G. Zhang, Y. Gao, *J. Biomater. Sci., Polym. Ed.* **2020**, *31*, 1041; b) D. A. Taylor, P.-F. Lee, Y. Barac, C. Hochman-Mendez, L. C. Sampaio, in *Emerging Technologies for Heart Diseases*, Elsevier, Udi Nussinovitch **2020**, pp. 291–310; c) Y. Seo, Y. Jung, S. H. Kim, *Acta Biomater.* **2018**, *67*, 270.
- [75] a) A. C. Daly, M. D. Davidson, J. A. Burdick, *Nat. Commun.* **2021**, *12*, 753; b) Z. Cesarz, K. Tamama, *Stem Cells Int.* **2016**, *2016*, 9176357.
- [76] B. Aldemir Dikici, F. Claeysens, *Front. Bioeng. Biotechnol.* **2020**, *8*, 875.
- [77] a) D. Bejleri, B. W. Streeter, A. L. Nachlas, M. E. Brown, R. Gaetani, K. L. Christman, M. E. Davis, *Adv. Healthcare Mater.* **2018**, *7*, 1800672; b) P. Jain, H. Kathuria, N. Dubey, *Biomaterials* **2022**, *287*, 121639; c) P.-H. Chang, H.-M. Chao, E. Chern, S.-H. Hsu, *Biomaterials* **2021**, *268*, 120575.
- [78] a) B. Subia, U. R. Dahiya, S. Mishra, J. Ayache, G. V. Casquillas, D. Caballero, R. L. Reis, S. C. Kundu, *J. Controlled Release* **2021**, *331*, 103; b) S. Nuciforo, M. H. Heim, *JHEP Rep.* **2021**, *3*, 100198; c) L. Zhang, F. Liu, N. Weygant, J. Zhang, P. Hu, Z. Qin, J. Yang, Q. Cheng, F. Fan, Y. Zeng, *Cancer Lett.* **2021**, *500*, 87.
- [79] a) A. Gebeyehu, S. K. Surapaneni, J. Huang, A. Mondal, V. Z. Wang, N. F. Haruna, A. Bagde, P. Arthur, S. Kutlehria, N. Patel, *Sci. Rep.* **2021**, *11*, 372; b) B. R. Groveman, N. C. Ferreira, S. T. Foliaki, R. O. Walters, C. W. Winkler, B. Race, A. G. Hughson, G. Zanusso, C. L. Haigh, *Sci. Rep.* **2021**, *11*, 5165; c) L. Qian, J. Tcw, *Int. J. Mol. Sci.* **2021**, *22*, 1203; d) A. S. Barros, A. Costa, B. Sarmiento, *Adv. Drug Delivery Rev.* **2021**, *170*, 386.
- [80] Y. Li, Q.-M. Pi, P.-C. Wang, L.-J. Liu, Z.-G. Han, Y. Shao, Y. Zhai, Z.-Y. Zuo, Z.-Y. Gong, X. Yang, *RSC Adv.* **2017**, *7*, 56108.
- [81] J. A. Hickman, R. Graeser, R. de Hoogt, S. Vidic, C. Brito, M. Gutekunst, H. van der Kuip, *Biotechnol. J.* **2014**, *9*, 1115.
- [82] Y. Imamura, T. Mukohara, Y. Shimono, Y. Funakoshi, N. Chayahara, M. Toyoda, N. Kiyota, S. Takao, S. Kono, T. Nakatsura, *Oncol. Rep.* **2015**, *33*, 1837.
- [83] S. Melissaridou, E. Wiechec, M. Magan, M. V. Jain, M. K. Chung, L. Farnebo, K. Roberg, *Cancer Cell Int.* **2019**, *19*, 16.
- [84] M. J. Bissell, M. A. LaBarge, *Cancer Cell* **2005**, *7*, 17.
- [85] M. Kapałczyńska, T. Kolenda, W. Przybyła, M. Zajączkowska, A. Teresiak, V. Filas, M. Ibbs, R. Bliźniak, Ł. Łuczewski, K. Lamperska, *Arch. Med. Sci.* **2018**, *14*, 910.
- [86] M. Yliperttula, B. G. Chung, A. Navaladi, A. Manbachi, A. Urtti, *Eur. J. Pharm. Sci.* **2008**, *35*, 151.
- [87] Y. Xia, G. M. Whitesides, *Annu. Rev. Mater. Sci.* **1998**, *28*, 153.
- [88] T. Thorsen, S. J. Maerkl, S. R. Quake, *Science* **2002**, *298*, 580.
- [89] a) D. J. Beebe, G. A. Mensing, G. M. Walker, *Annu. Rev. Biomed. Eng.* **2002**, *4*, 261; b) G. S. Fiorini, D. T. Chiu, *BioTechniques* **2005**, *38*, 429.
- [90] O. Nur, M. Willander, in *Miniaturized Biosensing Devices: Fabrication and Applications*, Springer Nature, Singapore **2022**, pp. 99–122.
- [91] P. Kim, K. W. Kwon, M. C. Park, S. H. Lee, S. M. Kim, K. Y. Suh, *Biochip J* **2008**, *2*, 1.
- [92] a) K. Raj M, S. Chakraborty, *J. Appl. Polym. Sci.* **2020**, *137*, 48958; b) Y. Xia, G. M. Whitesides, *Angew. Chem., Int. Ed.* **1998**, *37*, 550.
- [93] V. Mehta, S. N. Rath, *Bio-Des. Manuf.* **2021**, *4*, 311.
- [94] a) N. Bhattacharjee, A. Urrios, S. Kang, A. Folch, *Lab Chip* **2016**, *16*, 1720; b) H. N. Chan, Y. Chen, Y. Shu, Y. Chen, Q. Tian, H. Wu, *Microfluid. Nanofluid.* **2015**, *19*, 9.
- [95] a) H. Gong, B. P. Bickham, A. T. Woolley, G. P. Nordin, *Lab Chip* **2017**, *17*, 2899; b) L. P. Bressan, C. B. Adamo, R. F. Quero, D. P. de Jesus, J. A. da Silva, *Anal. Methods* **2019**, *11*, 1014.
- [96] H. Bruus, *Theoretical Microfluidics*, Vol. 18, Oxford University Press, Oxford **2008**.
- [97] S. Halldorsson, E. Lucumi, R. Gómez-Sjöberg, R. M. Fleming, *Biosens. Bioelectron.* **2015**, *63*, 218.
- [98] Y. Song, X. Zhao, Q. Tian, H. Liang, *Microfluidics: Fundamentals, Devices, and Applications*, Wiley, New York **2018**.
- [99] M.-H. Wu, S.-B. Huang, G.-B. Lee, *Lab Chip* **2010**, *10*, 939.
- [100] S. Takayama, J. C. McDonald, E. Ostuni, M. N. Liang, P. J. Kenis, R. F. Ismagilov, G. M. Whitesides, *Proc. Natl. Acad. Sci. USA* **1999**, *96*, 5545.
- [101] K. Sato, M. Tokeshi, T. Sawada, T. Kitamori, *Anal. Sci.* **2000**, *16*, 455.
- [102] S. K. Dertinger, D. T. Chiu, N. L. Jeon, G. M. Whitesides, *Anal. Chem.* **2001**, *73*, 1240.
- [103] S.-Y. Teh, R. Lin, L.-H. Hung, A. P. Lee, *Lab Chip* **2008**, *8*, 198.
- [104] A. Abou-Hassan, O. Sandre, V. Cabuil, *Angew. Chem., Int. Ed.* **2010**, *49*, 6268.
- [105] D. A. Bruzewicz, A. P. McGuigan, G. M. Whitesides, *Lab Chip* **2008**, *8*, 663.
- [106] P. Novo, F. Volpetti, V. Chu, J. P. Conde, *Lab Chip* **2013**, *13*, 641.
- [107] D. T. Chiu, N. L. Jeon, S. Huang, R. S. Kane, C. J. Wargo, I. S. Choi, D. E. Ingber, G. M. Whitesides, *Proc. Natl. Acad. Sci. USA* **2000**, *97*, 2408.
- [108] E. Gottwald, S. Giselbrecht, C. Augspurger, B. Lahni, N. Dambrowsky, R. Truckenmüller, V. Plotter, T. Gietzelt, O. Wendt, W. Pfleging, *Lab Chip* **2007**, *7*, 777.
- [109] A. Liu, M. Islam, N. Stone, V. Varadarajan, J. Jeong, S. Bowie, P. Qiu, E. K. Waller, A. Alexeev, T. Sulchek, *Mater. Today* **2018**, *21*, 703.
- [110] J. J. Agresti, E. Antipov, A. R. Abate, K. Ahn, A. C. Rowat, J.-C. Baret, M. Marquez, A. M. Klibanov, A. D. Griffiths, D. A. Weitz, *Proc. Natl. Acad. Sci. USA* **2010**, *107*, 4004.



- [111] L. Y. Yeo, H. C. Chang, P. P. Chan, J. R. Friend, *Small* **2011**, 7, 12.
- [112] X. Ren, P. Ghassemi, H. Babahosseini, J. S. Strobl, M. Agah, *ACS Sens.* **2017**, 2, 290.
- [113] A. L. Paguirigan, D. J. Beebe, *Integr. Biol.* **2009**, 1, 182.
- [114] Y. S. Heo, L. M. Cabrera, J. W. Song, N. Futai, Y.-C. Tung, G. D. Smith, S. Takayama, *Anal. Chem.* **2007**, 79, 1126.
- [115] A. L. Paguirigan, D. J. Beebe, *BioEssays* **2008**, 30, 811.
- [116] W. M. Saltzman, P. Parsons-Wingerter, K. W. Leong, S. Lin, *J. Biomed. Mater. Res.* **1991**, 25, 741.
- [117] S. K. Sia, G. M. Whitesides, *Electrophoresis* **2003**, 24, 3563.
- [118] E. Jastrzebska, A. Zuchowska, S. Flis, P. Sokolowska, M. Bulka, A. Dybko, Z. Brzozka, *Biomicrofluidics* **2018**, 12, 044105.
- [119] a) D. Bodas, C. Khan-Malek, *Sens. Actuators, B* **2007**, 123, 368; b) J. Fu, K. Y. Quek, Y. J. Chuah, C. S. Lim, C. Fan, D.-A. Wang, *J. Mater. Chem. B* **2016**, 4, 7961.
- [120] P. Xue, Q. Li, L. Sun, L. Zhang, Z. Xu, C. M. Li, Y. Kang, *Microfluid. Nanofluid.* **2018**, 22, 1.
- [121] a) R. Gomez-Sjoberg, A. A. Leyrat, B. T. Houseman, K. Shokat, S. R. Quake, *Anal. Chem.* **2010**, 82, 8954; b) J. D. Wang, N. J. Douville, S. Takayama, M. ElSayed, *Ann. Biomed. Eng.* **2012**, 40, 1862.
- [122] M. W. Toepke, D. J. Beebe, *Lab Chip* **2006**, 6, 1484.
- [123] B. Van Meer, H. de Vries, K. Firth, J. van Weerd, L. Tertoolen, H. Karperien, P. Jonkheijm, C. Denning, A. IJzerman, C. Mummery, *Biochem. Biophys. Res. Commun.* **2017**, 482, 323.
- [124] Z. Zhang, X. Feng, Q. Luo, B. F. Liu, *Electrophoresis* **2009**, 30, 3174.
- [125] Y. J. Chuah, S. Kuddannaya, M. H. A. Lee, Y. Zhang, Y. Kang, *Biomater. Sci.* **2015**, 3, 383.
- [126] L. Sun, Y. Luo, Z. Gao, W. Zhao, B. Lin, *Electrophoresis* **2015**, 36, 889.
- [127] H. Sasaki, H. Onoe, T. Osaki, R. Kawano, S. Takeuchi, *Sens. Actuators, B* **2010**, 150, 478.
- [128] C. F. Carlborg, T. Haraldsson, K. Öberg, M. Malkoch, W. van der Wijngaart, *Lab Chip* **2011**, 11, 3136.
- [129] G. Pardon, F. Saharil, J. M. Karlsson, O. Supekar, C. F. Carlborg, W. van der Wijngaart, T. Haraldsson, *Microfluid. Nanofluid.* **2014**, 17, 773.
- [130] J. Lam, R. A. Marklein, J. A. Jimenez-Torres, D. J. Beebe, S. R. Bauer, K. E. Sung, *SLAS Technol.: Transl. Life Sci. Innovation* **2017**, 22, 646.
- [131] K. Ziolkowska, E. Jedrych, R. Kwapiszewski, J. Lopacinska, M. Skolimowski, M. Chudy, *Sens. Actuators, B* **2010**, 145, 533.
- [132] S. B. Campbell, Q. Wu, J. Yazbeck, C. Liu, S. Okhovatian, M. Radisic, *ACS Biomater. Sci. Eng.* **2020**, 7, 2880.
- [133] Y.-s. Torisawa, B. Mosadegh, G. D. Luker, M. Morell, K. S. O'Shea, S. Takayama, *Integr. Biol.* **2009**, 1, 649.
- [134] Z. Wang, M.-C. Kim, M. Marquez, T. Thorsen, *Lab Chip* **2007**, 7, 740.
- [135] E. W. Young, D. J. Beebe, *Chem. Soc. Rev.* **2010**, 39, 1036.
- [136] C. K. Byun, K. Abi-Samra, Y. K. Cho, S. Takayama, *Electrophoresis* **2014**, 35, 245.
- [137] M. R. Behrens, H. C. Fuller, E. R. Swist, J. Wu, M. M. Islam, Z. Long, W. C. Ruder, R. Steward, *Sci. Rep.* **2020**, 10, 1543.
- [138] N. S. G. K. Devaraju, M. A. Unger, *Lab Chip* **2012**, 12, 4809.
- [139] X. Zhang, Z. Chen, Y. Huang, *Biomicrofluidics* **2015**, 9, 014118.
- [140] a) Y. Nakashima, T. Yasuda, *Sens. Actuators, A* **2007**, 139, 252; b) J. M. Lee, J. E. Kim, E. Kang, S. H. Lee, B. G. Chung, *Electrophoresis* **2011**, 32, 3133.
- [141] F. Wang, *Cold Spring Harbor Perspect. Biol.* **2009**, 1, a002980.
- [142] a) G. M. Walker, J. Sai, A. Richmond, M. Stremmer, C. Y. Chung, J. P. Wikswo, *Lab Chip* **2005**, 5, 611; b) F. Lin, C. M.-C. Nguyen, S.-J. Wang, W. Saadi, S. P. Gross, N. L. Jeon, *Ann. Biomed. Eng.* **2005**, 33, 475.
- [143] S. Schmidt, P. Friedl, *Cell Tissue Res.* **2010**, 339, 83.
- [144] a) B. Heit, S. Tavener, E. Raharjo, P. Kubes, *J. Cell Biol.* **2002**, 159, 91; b) V. V. Abhyankar, M. A. Lokuta, A. Huttenlocher, D. J. Beebe, *Lab Chip* **2006**, 6, 389.
- [145] a) S. A. Eccles, *Curr. Opin. Genet. Dev.* **2005**, 15, 77; b) B. Weigelt, J. L. Peterse, L. J. Van't Veer, *Nat. Rev. Cancer* **2005**, 5, 591; c) H.-C. Chiang, Y.-S. Wang, C.-H. Chou, A. T. Liao, R.-M. Chu, C.-S. Lin, *BMC Vet. Res.* **2012**, 8, 216.
- [146] E. Cukierman, R. Pankov, D. R. Stevens, K. M. Yamada, *Science* **2001**, 294, 1708.
- [147] C. Hu, J. Liu, H. Chen, F. Nie, *Biochem. Anal. Biochem.* **2017**, 6, 2161.
- [148] a) S. Feng, S. Mao, Q. Zhang, W. Li, J.-M. Lin, *ACS Sens.* **2019**, 4, 521; b) M. Wang, Y. Yang, L. Han, F. Xu, F. Li, *J. Cell. Physiol.* **2020**, 235, 4070.
- [149] A. Y. Shourabi, N. Kashaninejad, M. S. Saidi, *J. Sci.: Adv. Mater. Devices* **2021**, 6, 280.
- [150] S. Shen, X. Zhang, F. Zhang, D. Wang, D. Long, Y. Niu, *Talanta* **2020**, 208, 120477.
- [151] a) S. Shen, F. Zhang, S. Wang, J. Wang, D. Long, D. Wang, Y. Niu, *Sens. Actuators, B* **2019**, 287, 320; b) S. Shen, C. Tian, T. Li, J. Xu, S.-W. Chen, Q. Tu, M.-S. Yuan, W. Liu, J. Wang, *Lab Chip* **2017**, 17, 3578.
- [152] R. Lee, J. Lee, K.-B. Kim, J. Kim, *Photodiagn. Photodyn. Ther.* **2022**, 38, 102812.
- [153] M. Azizi, B. Davaji, A. V. Nguyen, S. Zhang, B. Dogan, K. W. Simpson, A. Abbaspourrad, *ACS Sens.* **2021**, 6, 1560.
- [154] M. Samandari, L. Rafiee, F. Alipanah, A. Sanati-Nezhad, S. H. Javanmard, *Sci. Rep.* **2021**, 11, 10310.
- [155] X. Lin, J. Su, S. Zhou, *Chin. Chem. Lett.* **2022**, 33, 3133.
- [156] H. Song, D. L. Chen, R. F. Ismagilov, *Angew. Chem., Int. Ed.* **2006**, 45, 7336.
- [157] a) D. T. Chiu, R. M. Lorenz, G. D. Jeffries, *Anal. Chem.* **2009**, 81, 5111; b) A. Otten, S. Köster, B. Struth, A. Snigirev, T. Pfohl, *J. Synchrotron Radiat.* **2005**, 12, 745; c) P. Watts, S. J. Haswell, *Curr. Opin. Chem. Biol.* **2003**, 7, 380; d) P. S. Dittrich, A. Manz, *Nat. Rev. Drug Discovery* **2006**, 5, 210.
- [158] a) P. Umbanhowar, V. Prasad, D. A. Weitz, *Langmuir* **2000**, 16, 347; b) A. S. Utada, E. Lorenceau, D. R. Link, P. D. Kaplan, H. A. Stone, D. Weitz, *Science* **2005**, 308, 537; c) C. N. Baroud, F. Gallaire, R. Dargatzoulis, *Lab Chip* **2010**, 10, 2032.
- [159] H. Song, J. D. Tice, R. F. Ismagilov, *Angew. Chem.* **2003**, 115, 792.
- [160] P. Zhu, L. Wang, *Lab Chip* **2017**, 17, 34.
- [161] K. Matula, F. Rivello, W. T. Huck, *Adv. Biosyst.* **2020**, 4, 1900188.
- [162] A. M. Klein, L. Mazutis, I. Akartuna, N. Tallapragada, A. Veres, V. Li, L. Peshkin, D. A. Weitz, M. W. Kirschner, *Cell* **2015**, 161, 1187.
- [163] F. Del Ben, M. Turetta, G. Celetti, A. Piruska, M. Bulfoni, D. Cesselli, W. T. Huck, G. Scoles, *Angewandte Chemie* **2016**, 128, 8723.
- [164] a) M. W. Bosenberg, J. Massagué, *Curr. Opin. Cell Biol.* **1993**, 5, 832; b) P. R. Baraniak, T. C. McDevitt, *Cell Tissue Res.* **2012**, 347, 701; c) D. Bosnakovski, M. Mizuno, G. Kim, S. Takagi, M. Okumura, T. Fujinaga, *Biotechnol. Bioeng.* **2006**, 93, 1152.
- [165] a) L. Bian, M. Guvendiren, R. L. Mauck, J. A. Burdick, *Proc. Natl. Acad. Sci. USA* **2013**, 110, 10117; b) L. Schukur, P. Zorlutuna, J. M. Cha, H. Bae, A. Khademhosseini, *Adv. Healthcare Mater.* **2013**, 2, 195.
- [166] K. Białkowska, P. Komorowski, M. Bryszewska, K. Miłowska, *Int. J. Mol. Sci.* **2020**, 21, 6225.
- [167] E. J. Lee, S. J. Park, S. K. Kang, G.-H. Kim, H.-J. Kang, S.-W. Lee, H. B. Jeon, H.-S. Kim, *Mol. Ther.* **2012**, 20, 1424.
- [168] H. F. Chan, Y. Zhang, Y.-P. Ho, Y.-L. Chiu, Y. Jung, K. W. Leong, *Sci. Rep.* **2013**, 3, 3462.
- [169] L. Yu, S. Grist, S. Nasser, E. Cheng, Y.-C. Hwang, C. Ni, K. Cheung, *Biomicrofluidics* **2015**, 9, 024118.
- [170] P. Sabhachandani, S. Sarkar, S. Mckenney, D. Ravi, A. M. Evens, T. Konry, *J. Controlled Release* **2019**, 295, 21.
- [171] L. A. Bawazer, C. S. McNally, C. J. Empson, W. J. Marchant, T. P. Comyn, Y. Niu, S. Cho, M. J. McPherson, B. P. Binks, A. deMello, *Sci. Adv.* **2016**, 2, e1600567.



- [172] F. Leal-Calderon, V. Schmitt, *Curr. Opin. Colloid Interface Sci.* **2008**, *13*, 217.
- [173] Y. Gao, C.-X. Zhao, F. Sainsbury, *J. Colloid Interface Sci.* **2021**, *584*, 528.
- [174] W. Postek, P. Garstecki, *Acc. Chem. Res.* **2022**, *55*, 605.
- [175] H. E. Parker, S. Sengupta, A. V. Harish, R. R. Soares, H. N. Joensson, W. Margulis, A. Russom, F. Laurell, *Sci. Rep.* **2022**, *12*, 3539.
- [176] C. Sun, L. Liu, L. Pérez, X. Li, Y. Liu, P. Xu, E. A. Boritz, J. I. Mullins, A. R. Abate, *Nat. Biomed. Eng.* **2022**, *6*, 1004.
- [177] L. Chen, D. Li, X. Liu, Y. Xie, J. Shan, H. Huang, X. Yu, Y. Chen, W. Zheng, Z. Li, *ACS Sens.* **2022**, *7*, 2170.
- [178] K. Iwai, M. Wehrs, M. Garber, J. Sustarich, L. Washburn, Z. Costello, P. W. Kim, D. Ando, W. R. Gaillard, N. J. Hillson, *Microsyst. Nanoeng.* **2022**, *8*, 31.
- [179] E. Sweet, B. Yang, J. Chen, R. Vickerman, Y. Lin, A. Long, E. Jacobs, T. Wu, C. Mercier, R. Jew, *Microsyst. Nanoeng.* **2020**, *6*, 92.
- [180] N. A. Dafale, U. P. Semwal, R. K. Rajput, G. Singh, *J. Pharm. Anal.* **2016**, *6*, 207.
- [181] X. Chen, H. Chen, D. Wu, Q. Chen, Z. Zhou, R. Zhang, X. Peng, Y.-C. Su, D. Sun, *Sens. Actuators, B* **2018**, *276*, 507.
- [182] a) E. Jastrzebska, S. Flis, A. Rakowska, M. Chudy, Z. Jastrzebski, A. Dybko, Z. Brzozka, *Microchim. Acta* **2013**, *180*, 895; b) E. Tekin, C. Beppler, C. White, Z. Mao, V. M. Savage, P. J. Yeh, *J. R. Soc., Interface* **2016**, *13*, 20160332.
- [183] P. Liu, L. Fu, Z. Song, M. Man, H. Yuan, X. Zheng, Q. Kang, D. Shen, J. Song, B. Li, *Analyst* **2021**, *146*, 5255.
- [184] J. L. Jameson, D. L. Longo, *Obstet. Gynecol. Surv.* **2015**, *70*, 612.
- [185] M. A. Lancaster, J. A. Knoblich, *Science* **2014**, *345*, 1247125.
- [186] a) A. Farkhondeh, R. Li, K. Gorshkov, K. G. Chen, M. Might, S. Rodems, D. C. Lo, W. Zheng, *Drug Discovery Today* **2019**, *24*, 992; b) M. S. Eliott, L. Barbar, P. J. Tesar, *Hum. Mol. Genet.* **2018**, *27*, R89.
- [187] G.-A. Kim, N. J. Ginga, S. Takayama, *Cell. Mol. Gastroenterol. Hepatol.* **2018**, *6*, 123.
- [188] I. Khan, A. Prabhakar, C. Delepine, H. Tsang, V. Pham, M. Sur, *Biomecrofluidics* **2021**, *15*, 024105.
- [189] I. Salmon, S. Grebenyuk, A. R. A. Fattah, G. Rustandi, T. Pilkington, C. Verfaillie, A. Ranga, *Lab Chip* **2022**, *22*, 1615.
- [190] M. Sharafeldin, T. Chen, G. U. Ozkaya, D. Choudhary, A. A. Molinolo, J. S. Gutkind, J. F. Rusling, *Biosens. Bioelectron.* **2021**, *171*, 112681.
- [191] H. M. Almughamsi, M. K. Howell, S. R. Parry, J. E. Esene, J. B. Nielsen, G. P. Nordin, A. T. Woolley, *Analyst* **2022**, *147*, 734.
- [192] L. Wei, G. Fang, Z. Kuang, L. Cheng, H. Wu, D. Guo, A. Liu, *Sens. Actuators, B* **2022**, *353*, 131085.
- [193] K. Choi, A. H. Ng, R. Fobel, A. R. Wheeler, *Annu. Rev. Anal. Chem.* **2012**, *5*, 413.
- [194] G. J. Shah, H. Ding, S. Sadeghi, S. Chen, R. M. van Dam, *Lab Chip* **2013**, *13*, 2785.
- [195] A. H. Ng, B. B. Li, M. D. Chamberlain, A. R. Wheeler, *Annu. Rev. Biomed. Eng.* **2015**, *17*, 91.
- [196] J. Zhai, C. Li, H. Li, S. Yi, N. Yang, K. Miao, C. Deng, Y. Jia, P.-I. Mak, R. P. Martins, *Lab Chip* **2021**, *21*, 4749.
- [197] Y. Zhang, Y. Liu, *Biosensors* **2022**, *12*, 330.
- [198] W. Du, L. Li, K. P. Nichols, R. F. Ismagilov, *Lab Chip* **2009**, *9*, 2286.
- [199] C.-W. Chang, C.-C. Peng, W.-H. Liao, Y.-C. Tung, *Analyst* **2015**, *140*, 7355.
- [200] X. Liu, X. Li, N. Wu, Y. Luo, J. Zhang, Z. Yu, F. Shen, *ACS Sens.* **2022**, *7*, 1977.
- [201] M. A. Catterton, A. G. Ball, R. R. Pompano, *Micromachines* **2021**, *12*, 993.
- [202] a) S. Nishat, A. T. Jafry, A. W. Martinez, F. R. Awan, *Sens. Actuators, B* **2021**, *336*, 129681; b) D. M. Cate, J. A. Adkins, J. Mettakoonpitak, C. S. Henry, *Anal. Chem.* **2015**, *87*, 19; c) Y. Xia, J. Si, Z. Li, *Biosens. Bioelectron.* **2016**, *77*, 774.
- [203] a) M. Monjezi, M. Rismanian, H. Jamaati, N. Kashaninejad, *Appl. Sci.* **2021**, *11*, 9418; b) K. W. Yong, J. R. Choi, J. Y. Choi, A. C. Cowie, *Int. J. Mol. Sci.* **2020**, *21*, 5816.
- [204] K. F. Lei, T.-K. Liu, N.-M. Tsang, *Biosens. Bioelectron.* **2018**, *100*, 355.
- [205] a) M. C. Sapp, H. J. Fares, A. C. Estrada, K. J. Grande-Allen, *Acta Biomater.* **2015**, *13*, 199; b) R. Derda, A. Laromaine, A. Mammoto, S. K. Tang, T. Mammoto, D. E. Ingber, G. M. Whitesides, *Proc. Natl. Acad. Sci. USA* **2009**, *106*, 18457; c) M. Su, L. Ge, S. Ge, N. Li, J. Yu, M. Yan, J. Huang, *Anal. Chim. Acta* **2014**, *847*, 1.
- [206] Y. Wu, Q. Gao, J. Nie, J.-Z. Fu, Y. He, *ACS Biomater. Sci. Eng.* **2017**, *3*, 601.
- [207] S. X. Fu, P. Zuo, B. C. Ye, *Biotechnol. J.* **2021**, *16*, 2000126.
- [208] Y. Zhang, S. Ge, J. Yu, *TrAC, Trends Anal. Chem.* **2016**, *85*, 166.
- [209] a) H. Bouaffif, A. Koubaa, P. Perré, A. Cloutier, *Composites, Part A* **2009**, *40*, 1975; b) C. Chen, B. T. Mehl, A. S. Munshi, A. D. Townsend, D. M. Spence, R. S. Martin, *Anal. Methods* **2016**, *8*, 6005.
- [210] P. Prabhakar, R. K. Sen, N. Dwivedi, R. Khan, P. R. Solanki, A. K. Srivastava, C. Dhand, *Front. Nanotechnol.* **2021**, *3*, 609355.
- [211] T. N. Q. Le, N. N. Tran, M. Escrivà-Geloch, C. A. Serra, I. Fisk, D. J. McClements, V. Hessel, *Chem. Soc. Rev.* **2021**, *50*, 11979.
- [212] W. Fen, W. Sien, G. Xilan, *Biophys. Reps* **2021**, *7*, 504.
- [213] F. Shen, W. Du, J. E. Kreutz, A. Fok, R. F. Ismagilov, *Lab Chip* **2010**, *10*, 2666.
- [214] A. T. Jafry, H. Lee, A. P. Tenggara, H. Lim, Y. Moon, S.-H. Kim, Y. Lee, S.-M. Kim, S. Park, D. Byun, *Sens. Actuators, B* **2019**, *282*, 831.



**Beatriz D. Cardoso** received her B.Sc. in genetics and biotechnology from the University of Trás-os-Montes and Alto Douro -UTAD and M.Sc. in biophysics and bionanosystems from the University of Minho-UM, Portugal. She is a Ph.D. candidate in materials engineering at UM. Her research is focused on developing multi-stimuli-responsive solid magnetoliposomes for drugs-controlled release in pathological areas under thermal, magnetic, and pH responsiveness. Her work also includes the evaluation of magnetoliposomes in a microfluidic cell culture platform, aiming to create new solutions for testing the effectiveness of new therapies.



**Elisabete M. S. Castanheira** is an assistant professor in the Physics Department, School of Science, University of Minho, Braga (Portugal). Her research is focused on the development of bionanosystems for health and environment, specifically drug delivery systems; magnetic and plasmonic nanoparticles; liposomes and magnetoliposomes; magnetogels, magnetolipogels and plasmonic lipogels. In this investigation, photophysical techniques are widely employed, using fluorescent-labeled lipids and fluorescent drugs. The main applications of the developed nanosystems are multimodal cancer therapy (chemotherapy/magnetic hyperthermia/phototherapy) and the controlled release of bioinspired synthetic insecticides.



**Senentxu Lanceros-Méndez** graduated in physics at the University of the Basque Country, Leioa, Spain. He obtained his Ph.D. at the Institute of Physics of the Julius-Maximilians-Universität Würzburg, Germany. From 1998 he has been at the Physics Department of the University of Minho, Portugal, where he is an associate professor (now, on leave). In January 2016 he joined the BCMaterials, Basque Center for Materials, Applications and Nanostructures, where he is research professor and scientific director. His work is focused on polymer-based smart materials for sensors and actuators, energy and biomedical applications.



**Vanessa F. Cardoso** received her M.Sc. and Ph.D. in biomedical engineering in 2008 and 2012, all from the University of Minho-UM, Portugal. Since 2017 she has been an invited assistant professor at UM. Since 2021, she has been an assistant researcher at the CMEMS-UMinho Research Center from UM. Her research work is focused on the development, processing, characterization, and validation of smart and (multi)functional materials. She is also actively working on the design and fabrication of microfluidic platforms for biomedical applications and green chemistry approaches.